

The effect of aerosol dynamics and gas-particle conversion on dry deposition of inorganic reactive nitrogen in a temperate forest

Genki Katata¹, Kazuhide Matsuda², Atsuyuki Sorimachi³, Mizuo Kajino⁴, and Kentaro Takagi⁵

¹Institute for Global Change Adaptation Science (ICAS), Ibaraki University, Ibaraki, 310-8512, Japan

²Tokyo University of Agriculture and Technology, 3-5-8 Saiwai-cho, Fuchu, Tokyo 183-8509, Japan

³Department of Radiation Physics and Chemistry, Fukushima Medical University, 1 Hikarigaoka, Fukushima, Fukushima 960-1295, Japan

⁴Meteorological Research Institute, Japan Meteorological Agency, Tsukuba, Ibaraki 305-0052, Japan

⁵Teshio experimental forest, Field Science Center for Northern Biosphere. Hokkaido University, Toikanbetsu, Horonobe, Hokkaido 098-2943, Japan

Correspondence: Genki Katata (genki.katata.mirai@vc.ibaraki.ac.jp)

Abstract. Although dry deposition has an impact on nitrogen status in the forest environments, the mechanism for high dry deposition rates of fine nitrate particles (NO_3^-) observed in forests remains unknown and is a potential source of error in chemical transport models. Here we modified a multi-layer land surface model coupled with dry deposition and aerosol dynamics processes for a temperate mixed forest in Japan, so that we carried out its first application to the ammonium nitrate (NH_4NO_3) gas-particle conversion (gpc) and aerosol water uptake of reactive nitrogen compounds. The processes of thermodynamics, kinetics, and dry deposition for mixed inorganic particles are modeled by a triple-moment modal method. The data of inorganic mass and size-resolved total number concentrations measured by filter-pack and electrical low pressure impactor in autumn was used for model input and numerical analysis. The model overall reproduces observed turbulent fluxes above the canopy and vertical micrometeorological profiles as our previous studies. The sensitivity tests with and without gpc demonstrated inorganic mass and size-resolved total number concentrations clearly changed within the canopy. The results also revealed that the within-canopy evaporation of NH_4NO_3 under dry conditions significantly enhances deposition flux for fine NO_3^- and NH_4^+ particles, while reducing deposition flux for nitric acid gas (HNO_3). As a result of evaporation of particulate NH_4NO_3 , the calculated daytime mass flux of fine NO_3^- over the canopy were 15 times higher in gpc" scenario than "no gpc" scenario. This increase caused high contribution of particle deposition flux to total nitrogen flux over the forest ecosystem (38 %), while the contribution of NH_3 was still large. A dry deposition scheme coupled with aerosol dynamics may be required to improve the predictive accuracy of chemical transport models for the surface concentration of inorganic reactive nitrogen.

1 Introduction

Dry deposition of inorganic reactive nitrogen gas (e.g., HNO_3 and NH_3) and particle (e.g., NO_3^- and NH_4^+) is one of the important pathways of nitrogen input into forest ecosystems. In East Asia, where air pollutant emissions continue to increase (EANET, 2016), although the importance of dry deposition of inorganic reactive nitrogen is suggested by prior studies by

indirect estimate studies (e.g., Pan et al., 2012; Li et al. 2013; Xu et al., 2015), direct measurement studies are still limited (Nakahara et al., 2019). Recent observational studies at forests revealed that dry deposition flux of inorganic reactive nitrogen of fine NO_3^- was markedly higher than that expected from theory (Takahashi and Wakamatsu, 2004; Yamazaki et al., 2015; Honjo et al., 2016; Sakamoto et al., 2018; Nakahara et al., 2019). As long as physical deposition processes are dominant, the deposition velocities of SO_4^{2-} and NO_3^- particles are expected to be similar because both species exist in the same sub-micron size range (e.g., Wolff et al., 2011). However, Sakamoto et al. (2018) showed observed deposition velocity of NO_3^- as high as those of HNO_3 at a temperate mixed forest, using the relaxed eddy accumulation method (Matsuda et al., 2015). Nakahara et al. (2019) also observed a higher concentration gradient of fine NO_3^- than of fine SO_4^{2-} at a cool-temperate forest, using a thermodynamic equilibrium model to explain this difference by evaporation of NH_4NO_3 particles in the NH_4NO_3 - NH_3 - HNO_3 triad within the canopy. Numerical studies of chemical transport models for the East Asian region have demonstrated that the models have overestimated total (gas + particle) nitrate concentration at many locations (Kajino et al., 2013; Shimadera et al., 2018; Morino et al., 2015; Sakurai et al., 2015). Despite the many uncertain factors (e.g., the emission inventory; grid resolution; chemistry, physics, dynamics, and deposition modules), Shimadera et al. (2014) demonstrated that the surface concentration of total nitrate could be reproduced by increasing dry deposition velocity of HNO_3 by a factor of twenty, in reference to past numerical studies. Hence, the deposition velocity of NO_3^- of fine particles and/or HNO_3 is among the major uncertainties in the chemical transport modeling.

Modeling studies for dry deposition have demonstrated the importance of NH_4NO_3 volatilization during dry deposition of gaseous and particulate nitrates (Brost et al., 1988; van Oss et al., 1998; Kramm and Dlugi, 1994), although the process itself has already been known in the atmospheric chemistry community for a long time (Seinfeld and Pandis, 2006). All these studies used the "big-leaf" concept for the canopy representation under steady-state and thermodynamic equilibrium assumptions, with chemical reaction rates provided by observational data. Nemitz and Sutton (2004) developed a more sophisticated model by introducing chemical timescales for a size-resolved particle, and showed that the thermodynamic gas-particle conversion of NH_4NO_3 (hereinafter referred as gpc) may explain the bi-directional fluxes observed above a Dutch heathland. However, several uncertainties remained in their model results due to uncertainties in empirical treatments of particle deposition and thermodynamic processes, and gas concentration assumed in equilibrium with the particle phase of pure NH_4NO_3 (Nemitz and Sutton, 2004). Meanwhile, the equilibration of aerosols with surrounding liquid water is also important in determining the thermodynamic equilibrium of aerosols (e.g., Fountoukis and Nenes, 2007). An accurate evaluation of the impact of the NH_4NO_3 - NH_3 - HNO_3 conversion within the canopy requires a process-based model that includes the thermodynamics of mixed inorganic aerosols, linking to gas-phase chemistry, while making no equilibrium assumption is required (Nemitz, 2015).

We here propose a new multi-layer land surface model coupled with dry deposition and aerosol dynamics (thermodynamics and kinetics of mixed inorganic aerosols) for forest environments. In aerosol dynamics modeling, the moment method is used to reduce computational cost and include general processes such as condensation, coagulation, below-cloud scavenging processes (e.g., Binkowski and Shankar, 1995), and dry deposition (Bae et al., 2009). These processes are implemented into a multi-layer atmosphere-SOIL-VEGETATION model (SOLVEG) that includes particle and fog droplet deposition and hygroscopic particle growth processes (Katata et al., 2014). We apply the model to a Japanese mixed forest for calibration and validation. Finally,

we use numerical experiments to examine the impacts of two key processes on dry deposition flux over the canopy; gas-particle conversion of inorganic nitrogen compounds and hygroscopic growth.

2 Model description

2.1 Model overview

60 A one-dimensional multi-layer model SOLVEG model consists of four sub-models: atmosphere, soil, vegetation, and radiation within the vegetation canopy. The general description for gas and particle transport and dry deposition is available in Katata and Ota (2017). In the atmosphere sub-model, one-dimensional diffusion equations are solved between atmospheric layers for horizontal wind speeds, potential temperature, specific (relative) humidity, liquid water content of the fog, turbulent kinetic energy and length scale (Katata, 2009), and gas and particle concentrations (Katata and Ota, 2017). Observational data are used
65 for the upper boundary conditions. Bulk transfer equations are applied at the lowest layer using the soil surface temperature and specific humidity calculated in the soil sub-model.

In the soil sub-model, the soil temperature, volumetric soil water content, and soil pore specific humidity are respectively predicted from heat conduction, mass balance in liquid water, and water vapor diffusion equations, respectively (Katata, 2009). Root water uptake is calculated from the transpiration rate in the vegetation sub-model. For soil CO₂, mass conservation
70 equations for liquid and gas phases are solved (Nagai, 2004). Organic matter dynamics are also considered (Ota et al., 2013); microbial decomposition and dissolved organic carbon (DOC) leaching in the above-ground litter layer, below-ground input of carbon from roots (root litter), and soil organic carbon (SOC) turnover and DOC transport along water flows throughout the soil profile for three SOC pools (active, slow, and passive) with different turnover times.

In the vegetation sub-model, profiles are predicted for leaf temperature, leaf surface water, and vertical liquid water flux
75 (Nagai, 2004). The heat budget equation at the leaf surface is solved to predict leaf temperature using key variables from the atmosphere sub-model combined with the radiation scheme. At the upper boundary of the sub-model, a given precipitation intensity is used for calculating vertical liquid water flux within the canopy based on the surface water budget equation. The CO₂ assimilation rate due to photosynthesis is predicted using Farquhar's formulations (Farquhar et al., 1980) and stomatal resistance. In the radiation sub-model, direct and diffuse downward and upward fluxes of solar and long-wave radiation are
80 calculated to obtain the radiation energy input at the canopy layers. Fractions of sunlit and shaded leaves at each canopy layer are adopted for the stomatal resistance and energy budget calculations.

A multi-layer snow module is unique in including the gravitational and capillary liquid water flows in the unsaturated snow layer based on van Genuchten's concept of water flow in the unsaturated zone (c.f., Hirashima et al., 2010; Katata et al., 2019). In the soil module, soil freeze-thaw processes based on the freezing-point depression equation are considered in heat conduction
85 and liquid water flow equations. Winter-related processes for grassland phenology, such as leaf development and senescence due to cold stresses, are also implemented in the vegetation sub-model. Carbon gain from photosynthesis and remobilized reserves are allocated among sinks based on changing sink priorities and strengths. Sink strengths are calculated based on the dynamics of leaves and stems and the acclimation to low temperature. The removal of tillers and leaves by cutting can be

simulated during the growing season, with subsequent regrowth of the sward. The regrowth rate after cutting is calculated at
 90 each phenological stage. Natural turnover of leaves and roots is modeled using typical life spans in years. Rooting depth and
 the fraction of roots in soil layers are modeled as functions of root biomass. Daily amounts of the dead root biomass (root litter)
 are used as inputs to SOC in the soil sub-model of SOLVEG.

2.2 Dry deposition

Since full descriptions for the dry deposition process of gases and particles are available in Katata et al. (2013; 2014) and
 95 Katata and Ota (2017), only the key equations are presented in the present subsection.

Using the compensation points for trace gases in the sub-stomatal cavity, χ_s (nmol m⁻³), and above the leaf water surface,
 χ_d (nmol m⁻³), we model bi-directional gas exchange fluxes with stomata, F_{gs} (nmol m⁻² s⁻¹), and with leaf water surfaces,
 F_{gd} (nmol m⁻² s⁻¹), for each canopy layer (Katata et al., 2013) as follows:

$$F_{gs} = a(D_{gas}/D_w)R'^{-1}[(r_b + r_d)\chi_s - r_b\chi_d - r_d\chi_a], \quad (1)$$

$$100 \quad F_{gd} = a(D_{gas}/D_w)R'^{-1}[(r_b + r_s)\chi_d - r_b\chi_s - r_s\chi_a], \quad (2)$$

where a is the leaf area density (m² m⁻³), D_{gas} and D_w are the diffusivities (m² s⁻¹) of trace gas and water vapor, r_b , r_s ,
 and r_d are the resistances (s m⁻¹) for leaf boundary layer, stomata, and the evaporation (cuticular), χ_a is the ambient gas
 concentration (nmol m⁻³) in the canopy layer, and $R' = (r_b r_s + r_b r_d + r_s r_d)$. The total gas exchange flux over the leaves can
 be calculated as the sum of F_{gs} and F_{gd} for all canopy layers. In accordance with a number of observations (e.g., Huebert and
 105 Robert, 1985), all χ_s , r_d , and r_s are set to be zero for highly reactive and water-soluble gas species of HNO₃ and HCl, i.e.,
 perfect absorption by plant canopies. For both species, the parameterization for a deciduous forest by Meyers et al. (1989) is
 used to calculate r_b . For NH₃, χ_s is calculated based on the thermodynamic equilibrium between NH₃ in the liquid and gas
 phases (Nemitz et al., 2000; Sutton et al., 1994):

$$\chi_s = \frac{161500}{T_c} \exp\left(\frac{10378}{T_c}\right) \Gamma_s, \quad (3)$$

110 where T_c is the canopy temperature (°C), Γ_s is the stomatal emission potential (also known as the apoplastic ratio) at 1013 hPa
 (Nemitz et al., 2004). Meanwhile, the NH₃ concentration at the leaf surface water (χ_d) is calculated by assuming Henrys Law
 and dissociation equilibrium with the atmospheric concentration of NH₃ at each canopy layer. To calculate the exchange flux
 of SO₂ and NH₃ over the wet canopy, the following empirical formula for r_d is applied (Massad et al., 2010):

$$r_d = 31.5AR^{-1} \exp[b(100 - RH)], \quad (4)$$

115 where b is the constant, RH is the relative humidity (%) and AR is the ratio of total acid/NH₃, represented as $(2[\text{SO}_2] + [\text{HNO}_3] + [\text{HCl}])/[\text{NH}_3]$
 at each atmospheric layer. The value of AR is determined from calculations of gaseous inorganic concentration
 at each atmospheric layer. Since the affinity (such as solubility on water) of SO₂ for the leaf surface is approximately twice
 that of NH₃ (van Hove et al., 1989), a half value of r_d calculated by Eq. (4) is applied to SO₂ deposition. The RH value could
 be affected by the leaf surface water content predicted at each canopy layer, based on water balance due to evaporation of leaf

120 surface water, interception of precipitation by leaves, capture of fog water by the leaves, and the drip from leaves (Katata et al., 2008; 2013). Since our model is not the dynamic modeling approach (e.g., Sutton et al., 1998; Flechard et al., 1999) to simulate NH₃ charging and discharging of the cuticle, Eq. (4) could have uncertainty at wet canopy in equilibrium with non-zero leaf surface concentration of NH₃.

The exchange flux of NH₃ over the ground (F_{g0}) was described with compensation points at the ground (chi_g) as

$$125 \quad F_{g0} = (D_{gas}/D_w)c_{H0}(\chi_{a0} - \chi_g), \quad (5)$$

$$\chi_g = \frac{161500}{T_{s0}} \exp\left(\frac{10378}{T_{s0}}\right) \Gamma_g, \quad (6)$$

where c_{H0} is the surface exchange coefficient for heat, χ_{a0} is the NH₃ concentration at the bottom of the atmospheric layer, T_{s0} is the soil surface temperature, and Γ_g is the emission potential at the ground surface.

As explained in Katata et al. (2014), the particle deposition rate F_p ($\mu\text{g m}^{-2} \text{s}^{-1}$ or $\# \text{m}^{-2} \text{s}^{-1}$) of each inorganic species
130 in each canopy layer is represented as

$$F_p = aE_p(D_p), \quad (7)$$

$$E_p = \varepsilon(D_p)F_f|\mathbf{u}|c_p(D_p), \quad (8)$$

where E_p is the capture of particles by leaves ($\mu\text{g m}^{-3} \text{s}^{-1}$ or $\# \text{m}^{-3} \text{s}^{-1}$); ε the total particle capture efficiency of plant leaves for particles by inertial impaction (Peters and Eiden, 1992), gravitational settling, Brownian diffusion (Kirsch and Fuchs, 1968),
135 and interception (Fuchs, 1964; Petroff et al., 2009); F_f is the shielding coefficient for particles in the horizontal direction; $|\mathbf{u}|$ the horizontal wind speed (m s^{-1}) at each canopy layer; and c_p is the mass or number concentration of particles ($\mu\text{g m}^{-3}$ or $\# \text{m}^{-3}$). E_p , ε , and c_p are integration values of given size bins with particle diameter (D_p [μm]).

2.3 Aerosol dynamics

In order to simulate changes in particle particle sizes due to condensation, evaporation, and water uptake, a triple-moment
140 modal method (Kajino et al., 2012) is employed at each atmospheric layer in SOLVEG. Particles are grouped into fine (accumulation) and Aitken mode with the size distribution prescribed by a lognormal function; while the coarse mode is not considered in the simulation. The lognormal function is identified by three parameters: number concentration (N [$\# \text{m}^{-3}$]), geometric mean diameter (D_g [μm]), and geometric standard deviation (σ_g). The triple-moment method predicts spatiotemporal changes in three moments (k) to identify the changes in the shape of each mode's lognormal size distribution. The selected
145 three moments are 0th, 2nd, and 3rd moments (M_0 , M_2 , and M_3), which are respectively number (N), surface area ($\text{m}^2 \text{m}^{-3}$), and volume concentrations ($\text{m}^3 \text{m}^{-3}$). D_g values for each moment are named D_{g0} , D_{g2} , and D_{g3} . The relationship of the above lognormal parameters and the three moments for each atmospheric layer are as follows:

$$M_k = ND_{g0}^k \exp\left[\frac{k^2}{2} \ln^2 \sigma_g\right], \quad (9)$$

$$D_{g0} = \left[\frac{M_2}{M_0}\right]^{\frac{3}{2}} \left[\frac{M_3}{M_0}\right]^{-\frac{3}{2}}, \ln^2 \sigma_g = -\ln\left[\frac{M_2}{M_0} \left(\frac{M_3}{M_0}\right)^{-\frac{2}{3}}\right]. \quad (10)$$

150 Particle growth is dynamically solved in the same manner of Kajino et al. (2012). The gas to particle mass transfer is driven by the difference between the current state and the thermodynamic equilibrium state, as simulated by ISORROPIA2 model (Fountoukis and Nenes, 2007) for semi-volatile inorganic components such as NO_3^- , NH_4^+ , Cl^- , and liquid water (H_2O). The gas-phase chemical production of HNO_3 could affect the simulated HNO_3 concentration and flux, which should be implemented to the model in future. The gas-particle conversion of organics is not considered in the present study because the
155 observational speciation data was not available. Thus, both organics and other components to total mass was assumed to be hydrophobic aerosols in the simulation. Since the current study focuses on change in mass gain/loss of accumulation mode aerosols, coagulation processes are not included in the simulation. Brownian coagulation is critically important for the prediction of number concentration of Aitken mode particles, but not very important for the prediction of accumulation mode particle mass (e.g., Kajino et al., 2013).

160 3 Simulation setup

3.1 Study site and observational data

We used the measurements at an observation tower in a mixed forest namely the Field Museum Tamakyuryo (FM Tama) of the Tokyo University of Agriculture and Technology, located in a western suburb of Tokyo, Japan ($35^\circ 38' \text{N}$, $139^\circ 23' \text{E}$). Deciduous tree species (*Quercus* spp.) are dominant around the meteorological tower along with some Japanese cedar (*Crytomeria japonica*). The canopy height around the tower is approximately 20 m. The growth period of deciduous trees is typically from
165 April to December. Site description details are provided by Matsuda et al. (2015) and Yamazaki et al. (2015).

Simulations were carried out in two experimental periods in the early autumn (26 September to 11 October 2016) and the late autumn (7 November to 7 December 2016). In the early autumn period, daytime (8:00-17:00 in local time) and nighttime (17:00-8:00 in local time) mean concentrations were available at five heights (1, 8, 16, 23, and 30 m) for inorganic gases, with
170 fine particle concentrations observed using a 4-stage filter-pack sampling system. System specifications were same as those of Nakahara et al. (2019) except for the particle filter material. This study used a glass fiber filter coated with Teflon for collecting fine and coarse particles. For the early autumn period, filter-pack sampling was continuously performed during the day and night except when it was raining. As a result, 5 daytime reading data sets and 6 nighttime reading data sets were available. The gaps between data in rain days of the early autumn period were linearly incorporated for simulations. Since the interpolation
175 could cause unrealistic effects on the results, we used only the calculations and measurements in the above no rain period for comparisons of inorganic mass concentration. For the late autumn period, the time resolution was relatively low as weekly continuous measurements. After the samples were collected, inorganic ions in each of the filters were extracted into deionized water by ultrasonic extraction, and then analyzed using ion chromatography (Dionex ICS-1100, Thermo Scientific).

In the only late autumn period, measurements of particle number concentrations were taken during the daytime (10:00-16:00)
180 for 7 days without rainfall. Airborne particle number concentrations were measured by an electrical low pressure impactor (ELPI+, Dekati Ltd.). In the ELPI+, sampled particles are charged by corona discharge and later separated by size using the principle of inertial classification in a 13-stage cascade low-pressure (40 hPa) impactor combined with a back-up filter stage.

During the collection process, the charged particles produce a current proportional to their respective number concentrations. The broad particle size distribution domain measured by the ELPI+ ranges from 6 nm to 10 μm . More details on the ELPI+ are described in Järvinen et al. (2014). The particle sample inlets for the ELPI+ were placed at heights of 30, 23, 17, 8, and 1 m at the tower through TYGON intake tubing of 7.94 mm inner diameter and respective lengths of 6, 5, 10, 20, and 25 m. Each sampling line for the 5 measuring heights was manually switched every two minutes. The transit times for particle samples in the tubing at each height ranged between 2 and 12 s. Results of the first minute of concentration measurement were rejected in order to avoid the mixing of air samples derived from different heights. All data were stored in a personal computer at a sampling rate of 1 s^{-1} . The raw data were averaged over intervals of 60 s and were later used for calculating 600 s mean vertical profiles. Particle penetration efficiencies of the sampling tubes were estimated using the indoor particles in the laboratory by changing the lengths of the sampling tubes (30, 20, 15, 10, and 5 m). Based on these results, the raw concentrations have been corrected prior to post-processing. Furthermore, the data were further screened out according to a few selection criteria to ensure their credibility with respect to three uncertainties in particular: uncertainty in number concentration measurements, signal to noise ratio (Deventer et al., 2015), and variation in background current (the signal obtained from particle-free air through a HEPA-filter for each particle stage) before and after the measurements.

Half-hourly meteorological data for horizontal wind speed, and air temperature and humidity at heights of 30, 25, 20, 10, 6, and 1 m at the tower were used for model input and validation. Incoming short-wave and long-wave radiation values at 30 m were used for model input, while incoming long-wave radiation was estimated by the parameterization of Duarte et al. (2006). Net radiation was measured using a net radiometer (Q7, REBS) and stored by a data-logger (CR10X, Campbell Scientific) as half-hourly means. A sonic anemometer (81000, Young) was used to measure the 3D wind velocities and air temperature, and an enclosed infrared $\text{CO}_2/\text{H}_2\text{O}$ gas analyzer (LI-7200, Li-Cor) was used to measure the molar fraction of CO_2 and H_2O . These data were sampled at a frequency of 10 Hz with the interface unit (LI-7550, Li-Cor). Half-hourly CO_2 , heat, and momentum fluxes were calculated using Eddy Pro software (ver. 4.2.0, Li-Cor), where double rotation (Kaimal and Finnigan, 1994) and block averaging were applied to the fluctuation data to calculate the covariances. We then corrected the effect of air density fluctuations on the flux values (Burba et al., 2012). Low-frequency losses (Moncrieff et al., 2004) and high-frequency losses for the low-pass filtering (Ibrom et al., 2007) and for the sensor separation (Horst and Lenschow, 2009) were corrected. All raw flux data were checked following the quality-control program proposed by Vickers and Mahrt (1997). Then we applied the quality check system proposed by Mauder and Foken (2006), and excluded data of low quality (qc-flag of 2).

The total (one-sided) leaf area index (LAI) measured with a plant canopy analyzer (LAI-2200, Li-cor) were 4.3 and 3.6 $\text{m}^2 \text{ m}^{-2}$ for October and November 2016, respectively. Vertical profiles of leaf area density (LAD) were provided in order to obtain the above values of total LAI by interpolated by gamma function interpolation, with the maximum at a height of 15 m following the way of Katata et al. (2013). LAI of the understory vegetation of 0.5 m in height was given as a typical value of $2.0 \text{ m}^2 \text{ m}^{-2}$ due to lack of observational data.

215 3.2 Boundary and initial conditions

The boundaries of the vegetation layers were set at heights of 0.05, 0.1, 0.2, 0.3, and 0.5 m (understory vegetation), and from 1 to 20 m (forest canopy) with an increment of 1 m, while atmospheric layers were extended from the 20 m canopy to 30 m with an increment of 1 m. Half-hourly data for precipitation, atmospheric pressure, horizontal wind speed, air temperature and humidity, and incoming long- and short-wave radiation were applied to the top atmospheric layer. Inorganic mass concentrations of gases (SO_2 , NH_3 , HNO_3 , and HCl) and PM2.5 particles (SO_4^{2-} , NO_3^- , NH_4^+ , Na^+ , Cl^- , Ca^{2+} , K^+ , Mg^{2+}) measured by filter-pack were linearly interpolated at half-hourly timescales. For Aitken mode, the inorganic mass concentration was assumed to be one-tenth of that of fine mode, based on size-resolved number concentrations from ELPI+ observations (not shown in figures). The boundaries of the soil layers were 0.02, 0.05, 0.1, 0.2, 0.5, 1.0, and 2.0 m in depth. Constant values for soil temperature (15 °C) and saturated volumetric water content for typical loam soil texture ($0.43 \text{ m}^3 \text{ m}^{-3}$) were taken. The model setup and parameters were provided in Table S1.

The boundary conditions and input data for simulation setup are summarized in Table 1. The lognormal parameter sets of (D_{g3} , σ_g) for fine and Aitken modes at the upper boundary condition were respectively set at (0.089 μm , 2.1) and (0.26 μm , 2.0) based on manual fitting of ELPI+ measurements at 30 m height (Fig. 1a). These parameter sets were applied to both the early and late autumn periods. In order to simulate the vertical profiles of total number concentration within the canopy, the volume fraction of inorganic compounds, f_{io} , was given by the data of total inorganic mass and total number concentration. For the late autumn period, temporal changes in weekly f_{io} values for fine and Aitken modes was given by the data of filter-pack and ELPI+ measurements. However, for the early autumn period, the ELPI+ measurements were unavailable as described in last subsection. Therefore, temporal changes in f_{io} (Fig. 1b) were set based on the filter-pack data at the study site and total PM2.5 mass concentrations observed at the nearest air quality monitoring station at Hachiouji (3 km west-north-west from the site). For both periods, f_{io} for Aitken mode was assumed to be the same as that for fine mode, since again no observational data were available.

Since no data were available in the study site for emission potentials of NH_3 at the ground surface (χ_g) and stomata (χ_s), we used typical values of $\Gamma_g = 300$ (Massad et al., 2010) and $\Gamma_s = 2000$ for forests (Neiryneck and Ceulemans, 2008).

In this study, we made a simulation with basic and less time-resolved datasets as very first application of the model to the NH_4NO_3 gas-particle conversion and aerosol water uptake of reactive nitrogen compounds. The above uncertainties associated with input data such as number concentration and particle size distribution should be improved in future.

3.3 Simulation scenarios

To reveal the impacts of each process of NH_4NO_3 gas-particle conversion and hygroscopic growth, the following four simulation scenarios were adopted: 1) NH_4NO_3 gas-particle conversion and aerosol water uptake ("gpc" scenario), 2) aerosol water uptake but no NH_4NO_3 gas-particle conversion ("no gpc" scenario), 3) NH_4NO_3 gas-particle conversion but no aerosol water uptake ("gpc dry" scenario), and 4) no NH_4NO_3 gas-particle conversion and no aerosol water uptake ("no gpc dry" sce-

nario). Calculations in all scenarios were compared with observations of vertical profiles of total number and inorganic mass concentrations within the canopy.

4 Results

250 4.1 Micrometeorology during autumn 2016

Temporal changes in friction velocity, net radiation, sensible and latent heat, and CO₂ flux over the canopy for the early autumn and the late autumn periods are shown in Figs. 2 and 3, respectively. Overall, the modeled momentum and heat fluxes agreed with observed values, while observed high values of friction velocity in November and December 2016 were slightly underestimated (Fig. 3a). Water vapor and CO₂ exchange processes that determine the level of stomatal uptake of gases were
255 also reproduced well by the model (Figs. 2 and 3; c and e).

Figures 4 and 5 illustrates time series for horizontal wind speed, air temperature, and relative humidity under the canopy in both simulation periods. Wind speed was underestimated within the forest, as was friction velocity (Fig. 3a and d), probably due to horizontal advection over the hilly terrain (Matsuda et al., 2015). For calculated air temperature and humidity, the primary determinants of ambient conditions of gas-particle conversion and aerosol hygroscopic growth, calculated temporal changes
260 were closed to the observations within the canopy (Figs. 3 and 4; b and c). The above features were found in mean vertical profiles during the daytime and nighttime (Fig. S1).

4.2 Inorganic mass concentration and flux in early autumn in 2016

Figure 6a and b shows time series for observed and calculated major inorganic nitrogen compounds (HNO₃ and NH₃ gases and NO₃⁻, and NH₄⁺ fine particles) under the canopy in the early autumn period. The difference between "gpc" and "no gpc" scenarios was substantial for HNO₃ and fine NO₃⁻ concentrations during the daytime on 28 September. In the "gpc" scenario,
265 HNO₃ concentration increased due to evaporation of NH₄NO₃ during the daytime, while NO₃⁻ concentration decreased. As a result, strong variations in NO₃⁻ mass concentration was reproduced in the "gpc" scenario. Less impact of evaporation of NH₄NO₃ on both NH₃ and fine NH₄⁺ concentrations was observed.

The calculated fine mode mass-based wet diameter (D_{g3}) and RH are shown in Fig. 6c. Hygroscopic growth has a large
270 impact on particle size distributions in comparisons between "no gpc" and "no gpc dry" scenarios; e.g., D_{g3} values in the latter were higher as 1.4 μm than those in the former as 0.4 μm during the nighttime on 29 September 2016. Although this process also influenced the size distribution during the daytime, competing shrinkage mechanism, NH₄NO₃ evaporation, appeared in the "gpc" scenario. As a result, the difference in daytime D_{g3} between "gpc" and "no gpc" scenarios was up to in 0.12 μm on 28 September.

275 Figure 7 depicts vertical profiles of normalized gaseous and particulate mass concentrations in the early autumn period. The model profiles averaged for only the sampling periods were compared with observed ones. In the "no gpc" scenario (Fig. 7b), vertical gradients of fine particle compounds (SO₄²⁻, NO₃⁻, and NH₄⁺) were similar, since the same equation for

collection efficiency of Eq. (8) was used for all inorganic particle compounds. In contrast, vertical gradients of NO_3^- and NH_4^+ concentrations drastically increased due to NH_4NO_3 evaporation in the "gpc" scenario (Fig. 7c and f), producing gradients similar to observed gradients (Fig. 7a and d). The above feature was also apparent in vertical profiles of mass flux for all inorganic nitrogen components during the daytime (Fig. S2). The impact of NH_4NO_3 evaporation was smaller during the nighttime (Fig. 7e) than the daytime (Fig. 7f), which also aligns with observed diurnal patterns (Fig. 7a and d). High values of observed fine SO_4^{2-} concentration were calculated in both scenarios (Fig. 7a-c).

Figure 8 shows time series for calculated apparent mass flux of HNO_3 , NH_3 , and fine NO_3^- and NH_4^+ over the canopy for "gpc" and "no gpc" scenarios. The actual deposition flux of each component by forest (ecosystem flux) was also shown for comparisons with apparent flux. The impact of NH_4NO_3 evaporation on fluxes was the highest from 26 to 29 September. Calculated NO_3^- flux above the canopy was positive during the nighttime for several days (Fig. 8c) due to condensation of HNO_3 (Fig. 8a). As is the case for in-canopy NH_3 concentration (Figs. 6 and 7), NH_4NO_3 evaporation has less impact on NH_3 flux than other species (Fig. 8b).

290 4.3 Particle size distribution in late autumn 2016

Figure 9 shows time series for number concentration within the canopy in the late autumn period, as well as parameters for a lognormal size distribution for fine mode. Initial number concentration values on 7 November (Fig. 9a) were tuned via adjustments of the ratio of inorganic compounds (f_{io}) for each mode. Below-canopy D_{g3} and σ_g were smaller in "gpc dry" than in "no gpc dry" due to NH_4NO_3 evaporation (Fig. 9b and d), while below-canopy D_{g0} was larger in "gpc dry" than in "no gpc dry" (Fig. 9c). In the "gpc" and "no gpc" scenarios in which aerosol water is considered, D_{g3} increased due to hygroscopic growth, while the influence of NH_4NO_3 gas-particle conversion on D_{g3} was still apparent (Fig. 9b). Some discrepancies between observations and calculations were found after 25 November 2016 in temporal changes in number concentration (Fig. 9a).

Figure 10 shows vertical profiles of parameters for a lognormal size distribution and normalized NO_3^- mass concentration in "no gpc" and "gpc" scenarios. For fine particles, values of D_{g3} and normalized NO_3^- concentration at 8 m were respectively 5.1 % and 8.9 % smaller in the "gpc" scenario than in the "no gpc" scenario due to evaporation of NH_4NO_3 (Fig. 8b and d), while calculated σ_g was also 1.2 % smaller (Fig. 8c). In contrast, calculated D_{g0} slightly increased 0.3 % at the same height (Fig. 19a). Almost no effect of NH_4NO_3 gas-particle conversion was found in Aitken mode (Fig. 10e-h).

Figure 11 shows the differences in the total number concentration among above, within, and below the canopy during the daytime in the late autumn period, with particular reference to the differences among these concentrations. In the sub-micron size range (0.1-0.4 μm), differences between height pairs were strong between 8 and 1 m (below), between 30 and 24 m (above), and between 24 and 8 m (within). In the "no gpc dry" scenario, the difference in number concentration between height pairs was minimal in the sub-micron size range as determined by modelled size-resolved dry deposition velocity (Fig. 11e). This is a similar result to demonstrated by past numerical study for size-resolved particle number flux (Ryder, 2010); the certain particle diameter around 0.15 μm at which the apparent flux switched from deposition to emission within the canopy and approximately reflected the peak in the number size distribution. Furthermore, the apparent emission flux was represented

as more particles shrink into a given size bin from the next larger size than are leaving the bin to the next smaller size, while more particles shrink out of a given size bin than shrink into it from the next larger size bin, resulting in apparent fast deposition (Ryder, 2010). In the "gpc" scenario (Fig. 11a-d), particles in fine mode shrunk in this size range due to in-canopy NH_4NO_3 evaporation, resulting in an apparent tendency to emit from the canopy to the air above (Fig. 11d). Meanwhile, differences in number concentration between 24 and 8 m (within) for large particles ($> 0.3 \mu\text{m}$) were excessively high in the "gpc" scenario compared to observational data. In the "no gpc" scenario, in which only aerosol water uptake was considered (Fig. 11c), fine particle size increased due to hygroscopic growth (Fig. 10), and the concentration differences between height pairs always remained positive in this range. Finally, if the "gpc" scenario, in which both processes of NH_4NO_3 evaporation and hygroscopic growth are considered (Fig. 11b), calculated negative gradients of number concentration appeared between 24 and 8 m (within) for the sub-micron range $0.1\text{-}0.4 \mu\text{m}$, again similar to the observed patterns (Fig. 11a).

5 Discussion

5.1 Uncertainties in observation and model results

SOLVEG reproduced the general features of gas concentration, fine particle mass, and fine particle number concentration observed within the canopy. Several uncertainties (e.g., low time resolution of weekly filter-pack data in the late autumn period; initialization of measurement uncertainty; complex topography of the study site) may cause underestimations in calculated wind speed (Figs. 3a and 4a) and overestimations in total number concentration within the canopy after 25 November 2016 (Fig. 9a). In Fig. 8, the conditions for NH_4NO_3 condensation were calculated in this forest, although these conditions are normally found over strong sources of NH_3 (e.g. Nemitz et al., 2009). Thus, the results from this study can only be considered a first test of the model to the NH_4NO_3 gas-particle conversion and aerosol water uptake of reactive nitrogen compounds, rather than a conclusive assessment of its capability.

Another uncertainty in the results could be associated with same composition assumption in size at the initial and boundary conditions. Variations of chemical composition in size caused variations in equilibrium vapor pressure at particle surface due to Kelvin and Raoult's effects, which caused uncertainty in the simulation of swelling and shrinking of particles. Since we used a modal aerosol dynamics method, differences of these effects within each mode cannot be resolved. We need to revisit this issue in the future by using size-resolved composition measurements and size-resolved aerosol model as done by Ryder (2010) to assess this uncertainty.

In the modeling aspect, particle growth due to biogenic secondary organics was not considered and might increase uncertainty in model results. Although this effect might not be important for dry deposition and evaporation of NH_4NO_3 that was the main focus of this study, this effect certainly influences the particle mass flux itself in the forest. Nevertheless, the order of the magnitude of observed normalized inorganic mass concentration within the canopy during the daytime, i.e., $\text{SO}_4^{2-} > \text{NH}_3 > \text{NH}_4^+ > \text{NO}_3^- > \text{HNO}_3$ (Fig. 7a) was well reproduced by the model in the "gpc" scenario (Fig. 7c). In the late autumn period, while there is no direct measurement of aerosol water content, the ambient RH profile that determines hygroscopic growth of aerosols was reproduced (Figs. 3c and 4c). As a result, the observed in-canopy negative gradient in number concentration

345 (i.e., apparent emission of particles) in 0.1-0.4 μm size range was simulated in the "gpc" scenario (Fig. 11a and b). These results indicate that the model results can likely be used to effectively address the impact of aerosol dynamics on dry deposition processes.

5.2 Formation mechanisms of particle size distributions

The complex form of the particle size distribution can be mainly explained by the combination of (1) effects of in-canopy
350 NH_4NO_3 evaporation of small particles and (2) fine mode hygroscopic growth of large particles. Observed vertical gradients of size-resolved number concentration within the canopy were reproduced only in the "gpc" scenario (Fig. 11b), although other scenarios showed different tendencies as follows (Fig. 11c-e). When only dry deposition processes were considered (Fig. 11e), number concentration above the canopy was always larger than that within the canopy. Although the sharp negative gradient of number concentration between height pairs was computed for the 0.1-0.4 μm size range when the gas-particle
355 conversion process was added to the model (Fig. 11d), positive gradients for large particles ($> 0.2 \mu\text{m}$) took on excessively high values compared to observational data. The number concentration of such large particles increased within the canopy due to hygroscopic growth (Fig. 11d and e), resulting in the negative gradient from the air above the canopy to the air within the canopy.

5.3 Impacts of gas-particle conversion and aerosol dynamics on dry deposition

360 To quantify the impact of gas-particle conversion of NH_4NO_3 on fine NO_3^- flux above the canopy, we plotted the respective ratios of HNO_3 , NO_3^- and NH_4^+ fluxes over the canopy in the "gpc" scenario (F_{gpc}) to those in the "no gpc" scenario (F_{nogpc}), plotting each such ratio against RH at the top of the canopy in the early autumn period (Fig. 12). In this study, since water uptake of aerosols, typically represented as the hygroscopic growth factor defined as the ratio between the humidified and dry particle diameters, is almost negligible under $RH < \text{approximately } 80 \%$ and increases over $RH > 80 \%$ (e.g., Fig. 6 in
365 Katata et al., 2014), we defined the threshold of 80 % for high and low RH conditions. As depicted in Fig. 12b, the gas-particle conversion of HNO_3 and NO_3^- shifted toward the particle phase under high RH conditions. Conversely, under low RH conditions ($< 80 \%$), most F_{gpc}/F_{nogpc} ratio values were higher than unity for fine NO_3^- concentration (Fig. 12b and e). The impact of NH_4NO_3 evaporation on fine NO_3^- flux was very strong just under the deliquescence relative humidity (DRH) of pure NH_4NO_3 of 61.8 %; the F_{gpc}/F_{nogpc} ratio reached ~ 40 around $RH = 50 \%$ (Fig. 12b). Notably, the thermodynamic equilibrium model in SOLVEG calculates the mutual DRH , which should not be pure NH_4NO_3 particles. Such high values of
370 (apparent) NO_3^- flux have been observed in various forest types in Europe, as summarized in Nemitz (2015). These cases may be also affected by NH_4NO_3 evaporation near the surface.

Calculated HNO_3 flux decreased with decreasing RH , due to evaporation of NH_4NO_3 (Fig. 12a). Most values of the F_{gpc}/F_{nogpc} ratio for HNO_3 under dry conditions ($RH < 80 \%$) were below 0.5, and even tended to be negative, i.e., emission
375 from the forest to the atmosphere. Prior studies have found this same flux difference; deposition velocity of HNO_3 varies in a range from 4 to 7 cm s^{-1} (Huebert and Robert, 1985; Meyers et al., 1989; Sievering et al., 2001). These velocities have often been found to be lower than theoretical maximum values or even negative, i.e., emission from the canopy (Pryor et al. 2002;

Nemitz et al., 2004). High HNO_3 concentrations were observed within the canopy with the appearance of upward HNO_3 flux over the canopy (Pryor et al., 2002), indicating the possibility of flux divergence due to NH_4NO_3 evaporation in the HNO_3 - NH_3 - NH_4NO_3 triad within the forest. This explanation has already been suggested by other studies (Harrison et al., 1989; Sutton et al., 1993; Kramm and Dlugi, 1994; Müller et al., 1993).

NH_4^+ flux over the forest was less influenced than NO_3^- by gas-to-particle conversion (Fig. 7c, f; Fig. 8d). It is because dry deposition rates of NH_3 were much lower than those of HNO_3 , and so differences in deposition rates between NH_3 and NH_4^+ are much smaller than those between HNO_3 and NO_3^- . In fact, the observed deposition trends for NH_3 and NH_4^+ were much weaker than those for HNO_3 and NO_3^- . Also, while the major counter-ion of NO_3^- was NH_4^+ , that of NH_4^+ was not NO_3^- but SO_4^{2-} . Even though same count of molecules of NH_3 and HNO_3 evaporated, the gross deposition rate of NH_4^+ appears to have been influenced mainly by $(\text{NH}_4)_2\text{SO}_4$ and/or NH_4HSO_4 as also suggested by Nemitz (2015). The effect of NH_4NO_3 gas-particle conversion on NH_3 flux was even lower than on fine NH_4^+ (Fig. 6a) because the mass concentration of NH_3 was much higher.

390 5.4 Influencing the chemical transport modeling

Once the gpc process is considered, particle deposition could have very important contribution as nitrogen flux over the forest ecosystem. Comparing the calculated daytime mass flux at 30 m height between "no gpc" and "gpc" scenarios in the early autumn period (Fig. S2), deposition flux of fine NO_3^- and NH_4^+ was 15 and 4 times higher in "gpc" scenario, respectively. Since there was almost no change in SO_4^{2-} flux between two scenarios, this change is only caused by gpc. For gas species, both HNO_3 and NH_3 slightly decreased to 0.6 and 0.8 times due to evaporation of NH_4NO_3 particles. This change in flux could be applied to that in deposition velocity of each species. Furthermore, although particle deposition flux contributes to only 5 % of total nitrogen flux above the canopy in "no gpc" scenario, this impact was increased to 38 % (NO_3^- : 27 %, NH_4^+ : 11 %) in "gpc" scenario. It should be noted that the contribution of NH_3 was still large as 37 % in total nitrogen flux even in the "gpc" scenario. The above results indicate that the increase of (apparent) particle deposition due to NH_4NO_3 evaporation may be important in the chemical transport modeling.

Theoretical values of deposition velocity for sub-micron particles typically ranging from $0.1\text{-}1\text{ cm s}^{-1}$ may have no substantial impact on surface concentrations in chemical transport models. However, as discussed in the previous subsection, high deposition velocity of fine NO_3^- due to evaporation in the forest (up to 40 times the above values) may effectively remove nitrate particles from the atmosphere over the forest and leeward. If the aerosol dynamics and gas-particle conversion processes can be incorporated into the dry deposition scheme in chemical transport models, we could improve upon or even eliminate prior studies' overestimates of the surface concentration of fine NO_3^- (Kajino et al., 2013; Shimadera et al., 2014, 2018; Morino et al., 2015; Sakurai et al., 2015). Hicks et al. (2016) found that in modeling deposition velocities of particles, the greatest uncertainty manifests in the range $0.1\text{-}1.0\ \mu\text{m}$. The cause of this uncertainty is still not convincingly established, although the differing treatments of some key particle deposition processes (e.g., turbulent diffusion) have been suggested by prior studies (Petroff and Zhang, 2010; Zhang and Shao, 2014). As demonstrated in Fig. 12b and c, evaporation of NH_4NO_3 under less humid conditions may play an important role for dry deposition of sub-micron particles.

6 Conclusions

A new multi-layer land surface model fully coupled with dry deposition and aerosol dynamics was developed to evaluate the impact of NH_4NO_3 - NH_3 - HNO_3 conversion in temperate forests. The model was applied to field studies of mass and number concentration profiles in a Japanese mixed forest during autumn 2016. Four model scenarios with/without NH_4NO_3 gas-particle conversion and/or aerosol water uptake were tested to quantify the impact of the above processes on dry deposition processes. The model overall successfully reproduced micrometeorological conditions (in particular, relative humidity) within and above the canopy. In the simulation including NH_4NO_3 gas-particle conversion processes, vertical gradients of normalized mass concentrations of nitrogen gases (HNO_3 and NH_3) and fine particles (NO_3^- and NH_4^+) within the canopy were clearly high than that for SO_4^{2-} . For particle size distribution, the observed emission tendency of total number concentration from the canopy to the atmosphere was explained by a larger effect of within-canopy evaporation of NH_4NO_3 than hygroscopic growth. As a result, the removal flux of calculated fine NO_3^- from the air above the forest to the forest can increase by up to 40 times under the DRH of pure NH_4NO_3 . Similarly, the removal flux of calculated fine NH_4^+ can increase up to ~ 10 times, though calculations for fine NH_4^+ fluctuate strongly with RH . Conversely, HNO_3 flux over the forest can decrease by 50 % or more due to NH_4NO_3 evaporation, as supported by prior studies. The processes of aerosol dynamics and NH_4NO_3 - NH_3 - HNO_3 conversion play a crucial role in the dry deposition of inorganic nitrogen particles in temperate forests. These processes can and should be incorporated into chemical transport models to improve the accuracy of total nitrate surface concentrations. An aerosol dynamics - dry deposition scheme simplified from that of this study can be implemented in chemical transport models.

Data availability. The output data in this study are publicly accessible via contacting the first author.

Author contributions. GK developed the model with support from MK, and performed the simulations using the data collected by KM, AS, and KT. GK prepared the manuscript with contributions from all co-authors.

Competing interests. We have no conflict of interest to declare.

Acknowledgements. We gratefully acknowledge the helpful comments and suggestions from Dr. Kentaro Hayashi at the National Institute for Agro-Environmental Sciences, Dr. Tatsuya Sakurai at Meisei University, Dr. Takeshi Izuta at Tokyo University of Agriculture and Technology, Dr. Satoru Miura at the Forestry and Forest Products Research Institute, and Drs. Makoto Tamura and Tetsuji Ito at Ibaraki University, Japan. Our thanks are also extended to Mr. Mao Xu at the Tokyo University of Agriculture and Technology, Japan, for his contribution to the filter-pack measurements. This work was partly supported by a Grant-in-Aid for Scientific Research (16H02933 and 17H01868) and Lead-

ing Initiative for Excellent Young Researchers, provided by the Japan Society for the Promotion of Science and the Ministry of Education, Culture, Sports, Science and Technology.

440 References

- Bae, S.Y., Jung, C.H., and Kim, Y.P.: Development of an aerosol dynamics model for dry deposition process using the moment method, *Aerosol. Sci. Technol.*, 43, 6, 570-580, 2009.
- Binkowski F. S., and Shankar, U.: The regional particulate model 1. Model description and preliminary results, *J. Geophys. Res.*, 100, D12, 26191-26209, 1995.
- 445 Brost, R.A., Delany, A.C., and Huebert, B.J.: Numerical modeling of concentrations and fluxes of HNO₃, NH₃, and NH₄NO₃ near the surface, *J. Geophys. Res.*, 93, 7137-7152, 1998.
- Burba, G., Schmidt, A., Scott, R.L., Nakai, T., Kathilankal, J., Fratini, G., Hanson, C., Law, B., McDermitt, D.K., Eckles, R., Furtaw, M., and Velgersdyk, M.: Calculating CO₂ and H₂O eddy covariance fluxes from an enclosed gas analyzer using an instantaneous mixing ratio, *Glob. Change Biol.*, 18, 385-399, 2012.
- 450 Deventer, M.J., Held, A., El-Madany, T.S., Klemm, O.: Size-resolved eddy covariance fluxes of nuclear to accumulation mode aerosol particles over a coniferous forest, *Agric. For. Meteorol.*, 214-215, 328-340, 2015.
- Duarte, H. F., Dias, N.L. and Maggioletto, S.R.: Assessing daytime downward longwave radiation estimates for clear and cloudy skies in southern Brazil, *Agric. For. Meteorol.*, 139, 171-181, 2006.
- EANET (Acid Deposition Monitoring Network in East Asia): The Third Periodic Report on the State of Acid Deposition in East Asia Part
455 III: Executive Summary, 2-5, https://www.eanet.asia/wp-content/uploads/2019/03/3_ex.pdf, 2016.
- Farquhar, G.D., Firth, P.M., Wetselaar, R. and Weir, B.: On the gaseous exchange of ammonia between leaves and the environment: determination of the ammonia compensation point, *Plant Physiol.*, 66, 710-714, 1980.
- Flechard, C., Fowler, D., Sutton, M.A. and Cape, J.N.: A dynamic chemical model of bi-directional ammonia exchange between semi-natural vegetation and the atmosphere, *Q. J. Roy. Meteorol. Soc.*, 125, 2611-2641.
- 460 Fowler, D., Pilegaard, K., Sutton, M.A., Ambus, P., Raivonen, M., Duyzer, J., Simpson, D., Fagerli, H., Fuzzi, S., Schjoerring, K.J., Granier, C., Nefter, A., Isaksen, I. S.A., Laj, P., Maione, M., and Monks, P.S.: Atmospheric composition change: Ecosystems-atmosphere interactions, *Atmos. Environ.*, 43, 5193-5267, 2009.
- Fountoukis, C., and Nenes, A.: ISORROPIA II: A computationally efficient thermodynamic equilibrium model for K⁺-Ca²⁺-Mg²⁺-NH₄⁺-Na⁺-SO₄²⁻-NO₃⁻-Cl⁻-H₂O aerosols, *Atmos. Chem. Phys.*, 7, 4639-4659, 2007.
- 465 Fuchs, N.A.: *The Mechanics of Aerosols*, Pergamon Press, Oxford, 408, 1964.
- Harrison, R.M., Rapsomanikis, S. and Turnbull, A.: Land Surface Exchange in a Chemically-Reactive System - Surface Fluxes of HNO₃, HCl and NH₃, *Atmos. Environ.*, 23, 1795-1800, 1989.
- Harrison, R.M., Sturges, W.T., Kitto, A.M.N. and Li, Y.: Kinetics of the evaporation of ammonium chloride and ammonium nitrate aerosols, *Atmos. Environ.*, 24A, 1883-1888, 1990.
- 470 Hicks, B. B., Saylor, R.D. and Baker, B.D.: Dry deposition of particles to canopies A look back and the road forward, *J. Geophys. Res. Atmos.*, 121, 14, 691-14, 707, doi:10.1002/2015JD024742., 2016.
- Honjo, T., Takahashi, A. and Matsuda, K.: Deposition velocity of sulfate and nitrate in PM_{2.5} above a forest in suburban Tokyo using relaxed eddy accumulation, *J. Jpn. Soc. Atmos. Environ.*, 51, 257-265, 2016 (in Japanese with English abstract).
- Huebert, B.J., Luke, W.T., Delany, A.C. and Brost, R.A.: Measurements of concentrations and dry surface fluxes of atmospheric nitrates in
475 the presence of ammonia, *J. Geophys. Res.*, 93, 7127-7136, 1988.

- Horst, T.W. and Lenschow, D.H.: Attenuation of scalar fluxes measured with spatially-displaced sensors, *Bound.-Layer Meteorol.*, 130, 275-300, 2009.
- Ibrom, A., Dellwik, E., Flyvbjerg, H., Jensen, N.O. and Pilegaard, K.: Strong low-pass filtering effects on water vapor flux measurements with closed-path eddy correlation systems, *Agric. For. Meteorol.*, 147, 140-156, 2007.
- 480 Järvinen, A., Aitoma, M., Rostedt, A., Keskinen, J., Yli-Ojanperä, J.: Calibration of the new electrical low pressure impactor (ELPI+), *J. Aerosol Sci.*, 69, 150-159, 2014.
- Kaimal, J.C. and Finnigan, J.J.: *Atmospheric boundary layer flows: their structure and measurement*, Oxford university press, 289, 1994.
- Kajino, M., Inomata, Y., Sato, K., Ueda, H., Han, Z., An, J., Katata, G., Deushi, M., Maki, T., Oshima, N., Kurokawa, J., Ohara, T., Takami, A. and Hatakeyama, S.: Development of an aerosol chemical transport model RAQM2 and predications of Northeast Asian aerosol mass, size, chemistry, and mixing type, *Atmos. Chem. Phys.*, 12, 11833-11856, 2012.
- 485 Kajino, M., Sato, K., Inomata, Y. and Ueda, H.: Source-receptor relationships of nitrate in Northeast Asia and influence of sea salt on the long-range transport of nitrate, *Atmos. Environ.*, 9, 67-78, 2013.
- Katata, G.: Improvement of a land surface model for accurate prediction of surface energy and water balances, *JAEA-Data/Code*, 2008-033, 64, 2009.
- 490 Katata, G., Nagai, H., Wrzesinsky, T., Klemm, O., Eugster, W., and Burkard, R.: Development of a land surface model including cloud water deposition on vegetation, *J. Appl. Meteorol. Climatol.*, 47, 21292146, 2008.
- Katata, G., Hayashi, K., Ono, K., Nagai, H., Miyata, A. and Mano, M.: Coupling atmospheric ammonia exchange process over a rice paddy field with a multi-layer atmosphere-soil-vegetation model, *Agric. For. Meteorol.*, 180, 1-21, 2013.
- Katata, G., Kajino, M., Matsuda, K., Takahashi, A. and Nakaya, K.: A numerical study of the effects of aerosol hygroscopic properties to dry deposition on a broad-leaved forest, *Atmos. Environ.*, 97, 501-510, 2014.
- 495 Katata, G. and Ota, M.: A terrestrial ecosystem model (SOLVEG) coupled with atmospheric gas and aerosol exchange processes, *JAEA-Data/Code*, 2016-014, 35, 2017.
- Katata, G., Grote, R., Mauder, M., Zeeman, M. and Ota, M.: Wintertime grassland dynamics may influence below-ground biomass under climate change: a model analysis, *Biogeosci.*, in press.
- 500 Kirsch, A. A. and Fuchs, N. A.: Studies on fibrous aerosol filters. III. Diffusional deposition of aerosols in fibrous filters, *Ann. Occup. Hyg.*, 11, 299-304, 1968.
- Kramm, G. and Dlugi, R.: Modelling of the vertical fluxes of nitric acid, ammonia and ammonium nitrate, *J. Atmos. Chem.*, 319-357, 1994.
- Li, K., Liu, X., Song, W., Chang, Y., Hu, Y., Tian, C.: Atmospheric nitrogen deposition at two sites in an arid environment of central Asia. *PLoS ONE*, 8, e67018, 2013.
- 505 Massad, R.-S., Nemitz, E. and Sutton, M.A.: Review and parameterisation of bi-directional ammonia exchange between vegetation and the atmosphere, *Atmos. Chem. Phys.*, 10, 10359-10386, 2010.
- Matsuda, K., Watanabe, I., Mizukami, K., Ban, S. and Takahashi, A.: Dry deposition of PM2.5 sulfate above a hilly forest using relaxed eddy accumulation, *Atmos. Environ.*, 107, 255-261, 2015.
- Mauder, M. and Foken, T.: Impact of post-field data processing on eddy covariance flux estimates and energy balance closure, *Meteorologische Zeitschrift*, 15, 597-609, 2006.
- 510 Moncrieff, J.B., Clement, R., Finnigan, J. and Meyers, T.: Averaging, detrending and filtering of eddy covariance time series, in *Handbook of micrometeorology: a guide for surface flux measurements*, eds. Lee, X., Massman, W.J., Law, B.E.. Kluwer Academic, Dordrecht, 7-31, 2004.

- Morino, Y., Nagashima, T., Sugata, S., Sato, K., Tanabe, K., Noguchi, T., Takami, A., Tanimoto, H. and Ohara, T.: Verification of chemical transport models for PM_{2.5} chemical composition using simultaneous measurement data over Japan, *Aerosol Air Qual. Res.*, 15, 2009-2023, 2015.
- Müller, H., Kramm, F. Meixner, Dollard, G.J., Fowler, D. and Possanzini, M.: Determination of HNO₃ dry deposition by modified Bowen ratio and aerodynamic profile techniques, *Tellus B*, 45, 346-367, 1993.
- Nagai, H.: Atmosphere-soil-vegetation model including CO₂ exchange processes: SOLVEG2, JAERI-Data/Code, 2004-014, 92, 2004.
- 520 Nakahara, S., Takagi, K., Sorimachi, A., Katata, G. and Matsuda, K.: Enhancement of dry deposition of PM_{2.5} nitrate in a cool-temperate forest, *Atmos. Environ.*, 212, 136-141, 2019.
- Nemitz, E., Sutton, M.A., Gut, A., José, R.S., Husted, S. and Schjoerring, J.K.: Sources and sinks of ammonia within an oilseed rape canopy, *Agr. Forest Meteorol.*, 105, 385-404, 2000.
- Nemitz, E. and Sutton, M.A.: Gas-particle interactions above a Dutch heathland: III. Modelling the influence of the NH₃-HNO₃-NH₄NO₃ equilibrium on size-segregated particle fluxes, *Atmos. Chem. Phys.*, 4, 1025-1045, 2004.
- 525 Nemitz, E., Sutton, M.A., Schjoerring, J.K., Husted, S. and Wyers, G.P.: Resistance modelling of ammonia exchange over oilseed rape, *Agr. Forest Meteorol.*, 105, 405-425, 2000.
- Nemitz, E., Sutton, M.A., Wyers, G.P. and Jongejan, P.A.C.: Gas-particle interactions above a Dutch heathland. I. Surface exchange fluxes of NH₃, SO₂, HNO₃ and HCl, *Atmos. Chem. Phys.* 4, 989-1005, 2004.
- 530 Nemitz, E., Dorsey, J. R., Flynn, M. J., Gallagher, M. W., Hensen, A., Erisman, J.-W., Owen, S. M., Dämmgen, U., and Sutton, M. A.: Aerosol fluxes and particle growth above managed grassland, *Biogeosci.*, 6, 1627-1645, 2009.
- Nemitz, E.: Surface/atmosphere Exchange of Atmospheric Acids and Aerosols, Including the Effect and Model Treatment of Chemical Interactions. Review and Integration of Biosphere-Atmosphere Modelling of Reactive Trace Gases and Volatile Aerosols, Springer, 115-149, 2015.
- 535 Neiryneck, J., and Ceulemans, R.: Bidirectional ammonia exchange above a mixed coniferous forest, *Environ. Pollut.*, 154, 424-438, 2008.
- Ota, M., Nagai, H. and Koarashi, J.: Root and dissolved organic carbon controls on subsurface soil carbon dynamics: A model approach, *J. Geophys. Res.*, 118, 1646-1659, 2013.
- Pan, Y., Wang, Y., Tang, G., and Wu, D.: Wet and dry deposition of atmospheric nitrogen at ten sites in Northern China, *Atmos. Chem. Phys.*, 12, 6515-6535, 2012.
- 540 Peters, K. and Eiden, R.: Modelling the dry deposition velocity of aerosol particles to a spruce forest, *Atmos. Environ.*, 26A, 2555-2564, 1992.
- Petroff, A., Zhang, L., Pryor, S.C. and Belot, Y.: An extended dry deposition model for aerosols onto broadleaf canopies, *J. Aerosol Sci.* 40, 218-240, 2009.
- Petroff, A. and Zhang, L.: Development and validation of a size-resolved particle dry deposition scheme for application in aerosol transport models, *Geosci. Model Dev.*, 3, 753-769, 2010.
- 545 Pryor, S.C., Barthelmie, R.J., Jensen, B., Jensen, N.O. and Sørensen, L.L.: HNO₃ fluxes to a deciduous forest derived using gradient and REA methods, *Atmos. Environ.*, 36, 5993-5999, 2002.
- Ryder, J., 2010. Emission, deposition and chemical conversion of atmospheric trace substances in and above vegetation canopies. PhD Thesis, University of Manchester, UK. Available from the University or via <https://nora.nerc.ac.uk>

- 550 Sakamoto, T., Nakahara, A., Takahashi, A., Sorimachi, A., Katata, G. and Matsuda, K.: Deposition velocity of PM_{2.5} nitrate and gaseous nitric acid above a forest in suburban Tokyo using relaxed eddy accumulation with denuder sampling technique, *J. Jpn. Soc. Atmos. Environ.*, 53, 136-143, 2018 (in Japanese with English abstract).
- Sakurai, T., Satake, S. and Matsuda, K.: Measurement of the inorganic ions in PM_{2.5} at western Tokyo and the evaluation for AQM performance based on the measurement, *Earozoru Kenkyu*, 30, 134-141, 2015 (In Japanese with English abstract).
- 555 Seinfeld, J.H. and Pandis, S.N.: *Atmospheric Chemistry and Physics: From Air Pollution to Climate Change*. 2nd eds., John Wiley & Sons, New York, 2006.
- Shimadera, H., Hayami, H., Chatani, S., Morino, Y., Mori, Y., Morikawa, T., Yamaji, K. and Ohara, T.: Sensitivity analyses of factors influencing CMAQ performance for fine particulate nitrate, *J. Air Waste Manage. Assoc.*, 64, 374-387, 2014.
- Shimadera, H., Hayami, H., Chatani, S., Morikawa, T., Morino, Y., Mori, Y., Tamaji, K., Nakatsuka, S. and Ohara, T.: Urban air quality
560 model inter-comparison study (UMICS) for improvement of PM_{2.5} simulation in greater Tokyo area of Japan, *Asian J. Atmos. Environ.*, 12, 139-152, 2018.
- Sievering, H., Enders, G., Kins, L., Kramm, G., Ruoss, K., Roider, G., Zelger, M., Anderson, I. and Dlugi, R.: Nitric acid, particulate nitrate and ammonium profiles at the Bayerisher Wald: evident for large deposition rates of total nitrate, *Atmos. Environ.*, 28, 311-315, 1994.
- Sutton, M.A., Asman, W.A.H. and Schjörriing, J.K.: Dry deposition of reduced nitrogen, *Tellus B* 46, 255-273, 1994
- 565 Sutton, M.A., Pitcairn, C.E.R. and Fowler, D.: The exchange of ammonia between the atmosphere and plant communities, *Adv. Ecol. Res.*, 24, 301-393, 1993.
- Sutton, M.A., Burkhardt, J.K., Guerin, D., Nemitz, E., and Fowler, D.: Development of resistance models to describe measurement of bi-directional ammonia surface atmosphere exchange, *Atmos. Environ.*, 32, 473-480, 1998.
- Takahashi, A. and Wakamatsu, T.: Estimation of deposition velocity of particles to a forest using the concentration gradient method, *J. Jpn. Soc. Atmos. Environ.*, 39, 53-61, 2004 (In Japanese with English abstract).
- van Hove, L.W.A., Adema, E.H. and Vredenberg, W.J.: A study of the adsorption of NH₃ and SO₂ on leaf surfaces, *Atmos. Environ.*, 23, 1479-1486, 1989.
- van Oss, R., Duyzer, J., and Wyers, P.: The influence of gas-to-particle conversion on measurements of ammonia exchange over forest, *Atmos. Environ.*, 32, 465-471, 1998.
- 575 Vickers, D. and Mahrt, L.: Quality control and flux sampling problems for tower and aircraft data, *J. Atmospheric Ocean. Technol.*, 14, 512-526, 1997.
- Wolff, V., Meixner, F.X. and Trebs, I.: Mixing ratios and exchange processes of the ammonia-nitric acid-ammonium nitrate triad above a spruce forest canopy. In: H. LacosteFrancid (Ed.), *Earth Observations for Land-Atmosphere Interaction Science*. European SpaceAgency, ESTEC PO Box 299 2200, 2011.
- 580 Xu, W., Luo, X. S., Pan, Y. P., Zhang, L., Tang, A. H., Shen, J. L., Zhang, Y., Li, K. H., Wu, Q. H., Yang, D. W., Zhang, Y. Y., Xue, J., Li, W. Q., Li, Q. Q., Tang, L., Lv, S. H., Liang, T., Tong, Y. A., Liu, P., Zhang, Q., Xiong, Z. Q., Shi, X. J., Wu, L. H., Shi, W. Q., Tian, K., Zhong, X. H., Shi, K., Tang, Q. Y., Zhang, L. J., Huang, J. L., He, C. E., Kuang, F. H., Zhu, B., Liu, H., Jin, X., Xin, Y. J., SHi, X. K., Du, E. Z., Dore, A. J., Tang, S., Collett, J. L., Jr, Goulding, K., Sun, Y. X., Ren, J., Zhang, F. S., and Liu, X. J.: Quantifying atmospheric nitrogen deposition through a nationwide monitoring network across China, *Atmos. Chem. Phys.*, 15, 12345-12360, 2015.
- 585 Yamazaki, T., Takahashi, A. and Matsuda, K.: Differences of dry deposition between sulfate and nitrate in PM_{2.5} to a forest in suburban Tokyo by vertical profile observations, *J. Jpn. Soc. Atmos. Environ.*, 50, 167-175, 2015 (In Japanese with English abstract).

- Zhang, Q., Jimenez, J.L., Canagaratna, M.R., D. Allan, J.D., Coe, H., Ulbrich, I., Alfarra, M., Takami, A., Middlebrook, A.M., Sun, Y.L., Dzepina, K., Dunlea, E., Docherty, K., DeCarlo, P., Salcedo, D., Onasch, T., Jayne, J.T., Miyoshi, T., Shimojo, A. and Worsnop, D.: Ubiquity and dominance of oxygenated species in organic aerosols in anthropogenically influenced Northern Hemisphere midlatitudes, *Geophys. Res. Lett.*, 34, L13801, doi:10.1029/2007GL029979, 2007.
- 590 Zhang, J. and Shao, Y.: A new parameterization of particle dry deposition over rough surfaces, *Atmos. Chem. Phys.*, 14, 12429-12440, 2014.

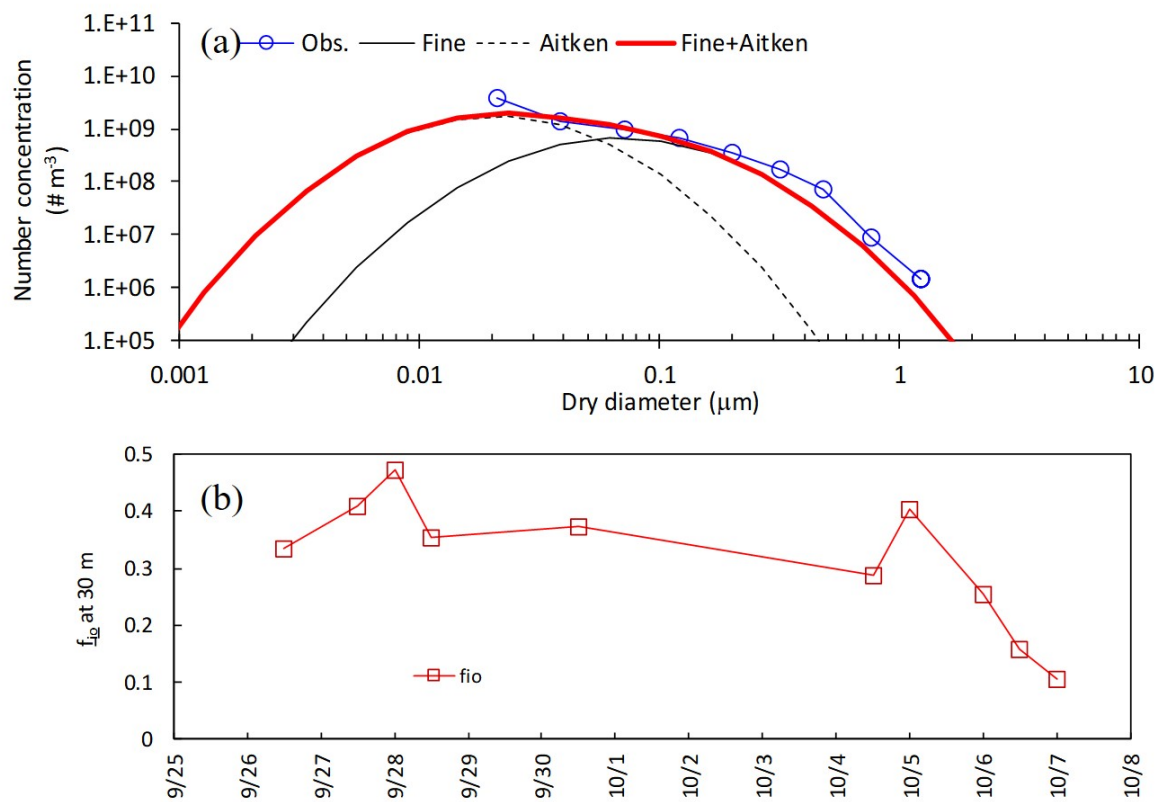


Figure 1. (a) Modeled and observed number-based size distribution of particles at 10:00 on 7 November 2016, and (b) temporal changes in the volume fraction of inorganic compounds (f_{io}) in the early autumn period.

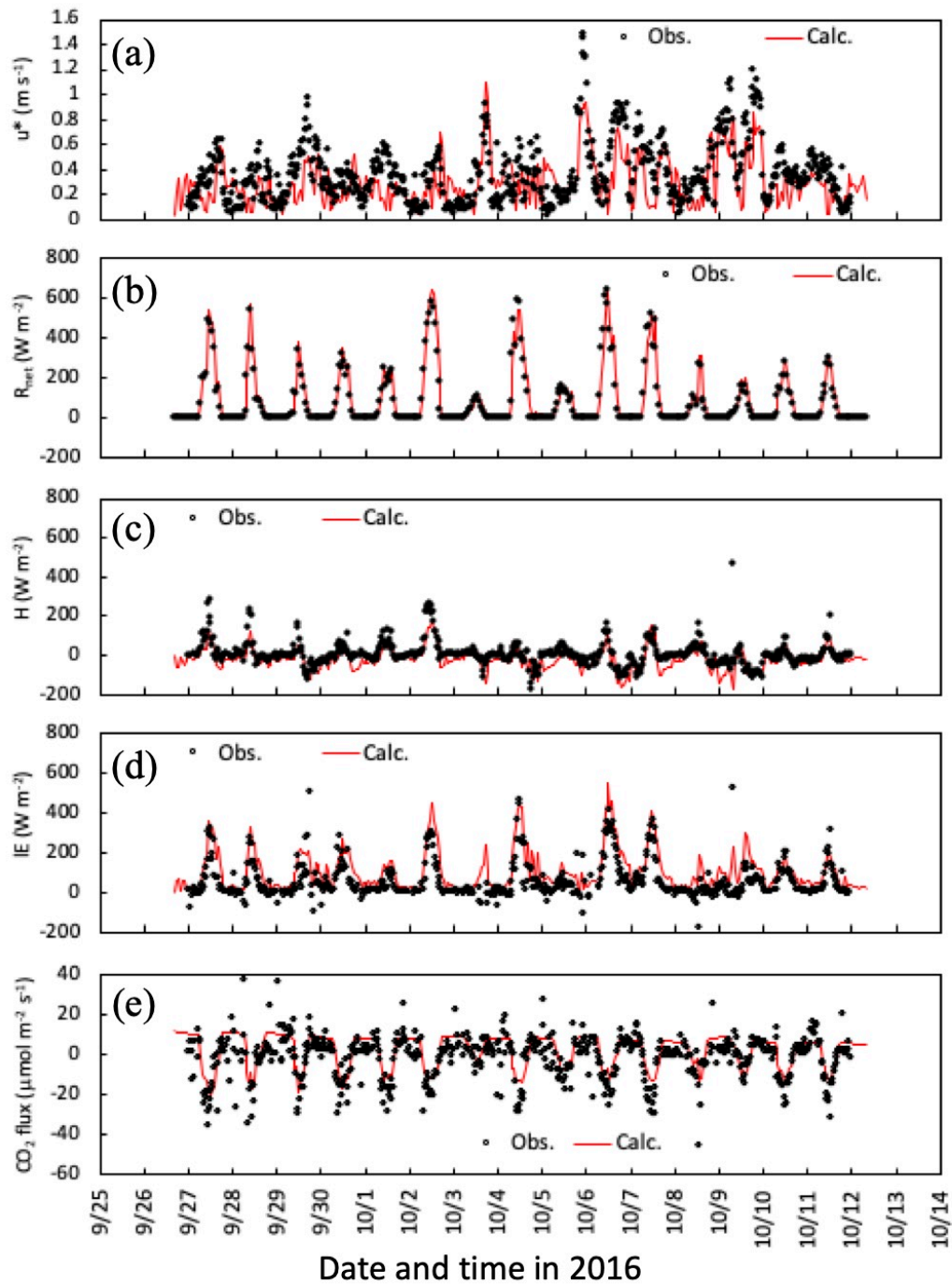


Figure 2. Temporal changes in observed and simulated (a) friction velocity, (b) net radiation, (c) sensible and (d) latent heat, and (e) CO_2 fluxes from 27 September to 11 October 2016.

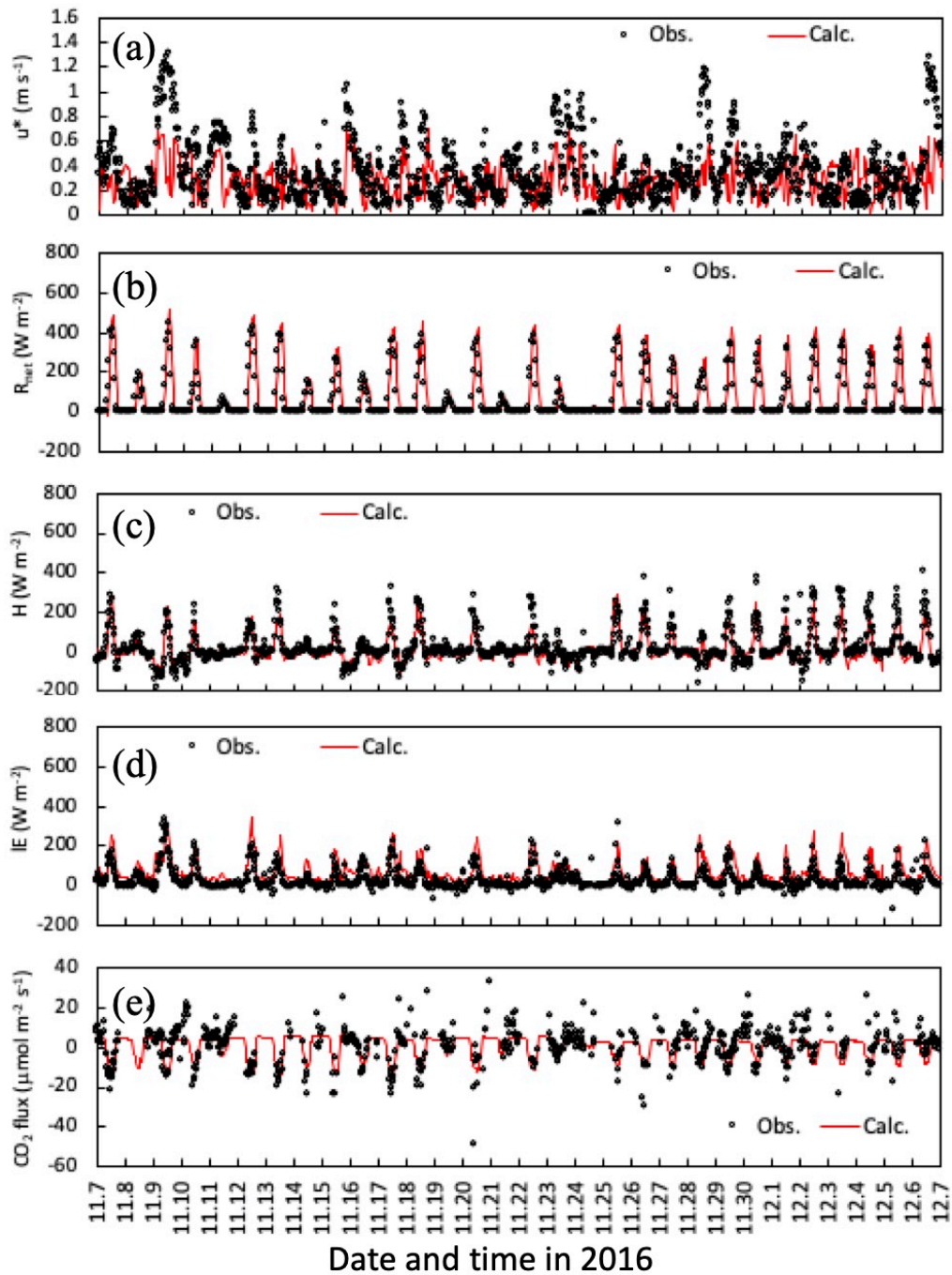


Figure 3. Temporal changes in observed and simulated (a) friction velocity, (b) net radiation, (c) sensible and (d) latent heat, and (e) CO_2 fluxes from 7 November to 6 December 2016.

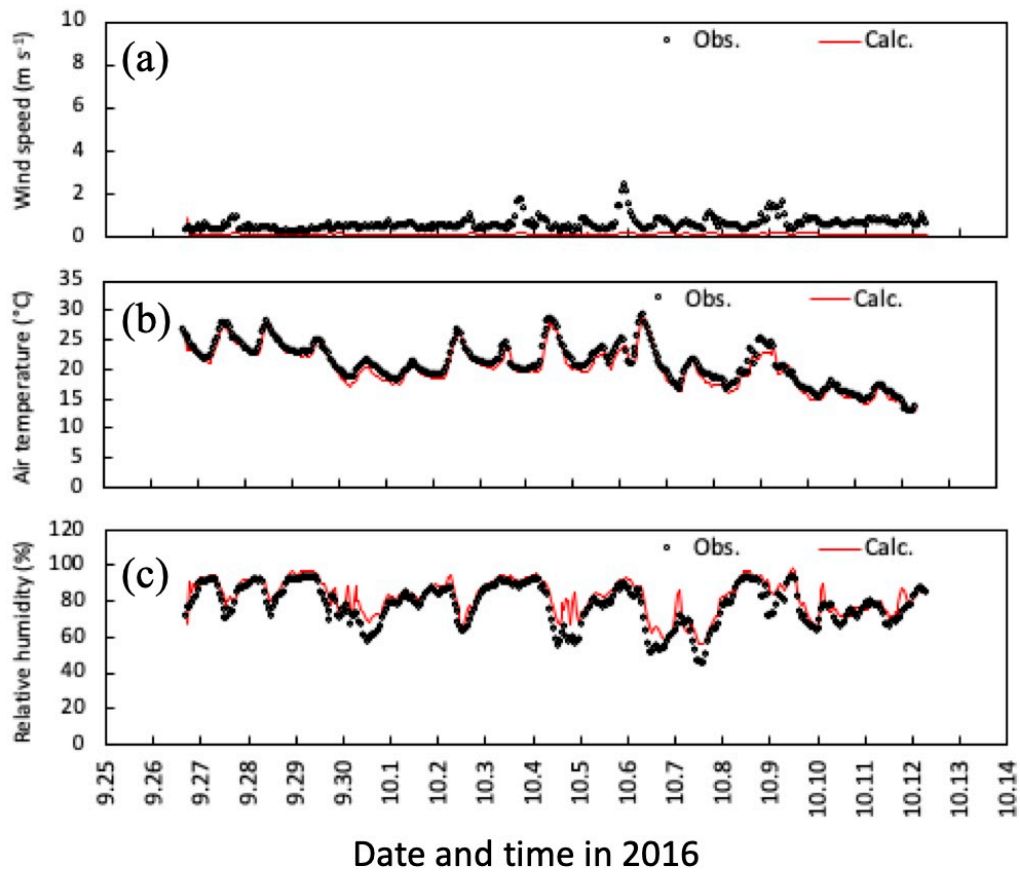


Figure 4. Temporal changes in observed and simulated (a) horizontal wind speed, (b) air temperature, and (c) relative humidity at 6 m height from 27 September to 11 October 2016.

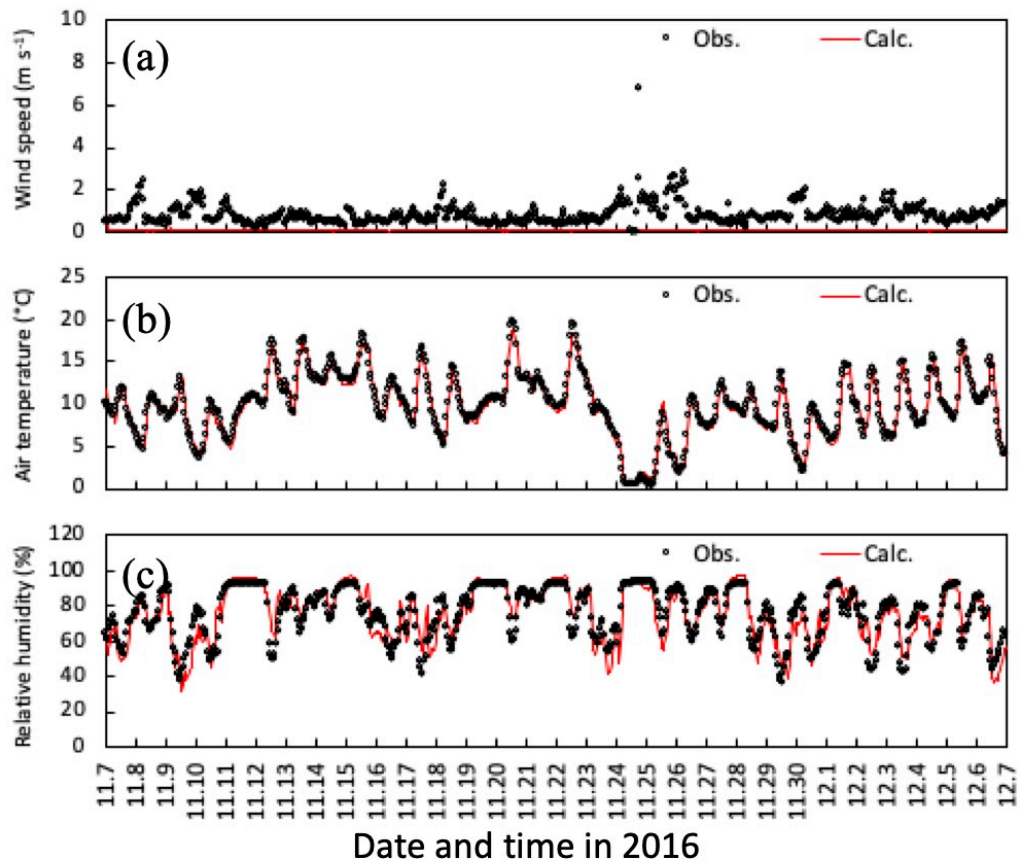


Figure 5. Temporal changes in observed and simulated (a) horizontal wind speed, (b) air temperature, and (c) relative humidity at 6 m height from 7 November to 6 December 2016

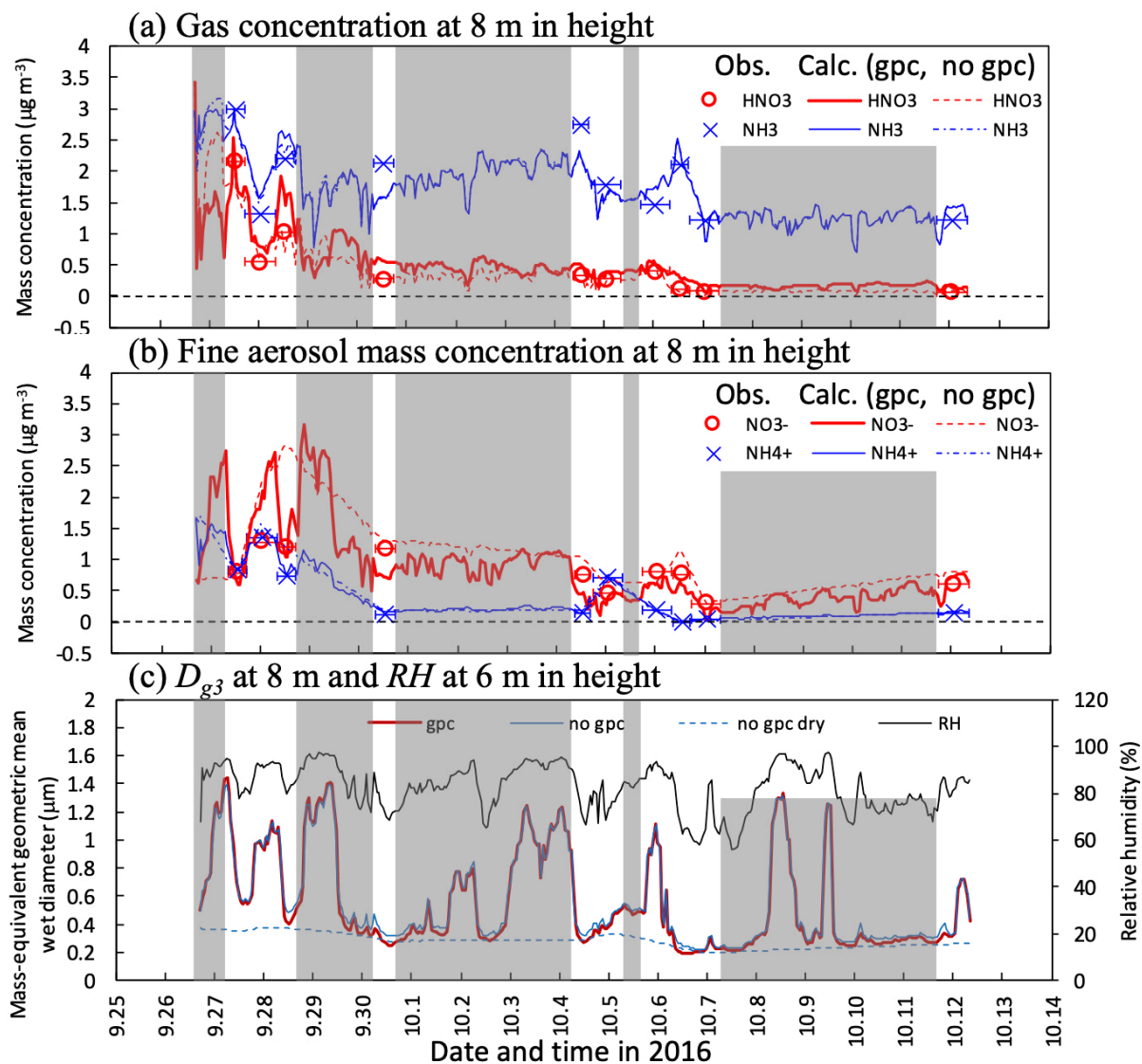


Figure 6. Temporal changes in observed and calculated mass concentrations of (a) HNO_3 and NH_3 gases and (b) NO_3^- and NH_4^+ fine particles, and mass-equivalent geometric mean wet diameter (D_{g3}) at 8 m height from 27 September to 11 October 2016. Calculations for three scenarios ("gpc", "no gpc", and "no gpc dry") are plotted in the figure. Calculated relative humidity (RH) at 6 m height in Fig. 3c also appears in (c). Grey shaded areas represent the rain period in which no filter-pack data were available.

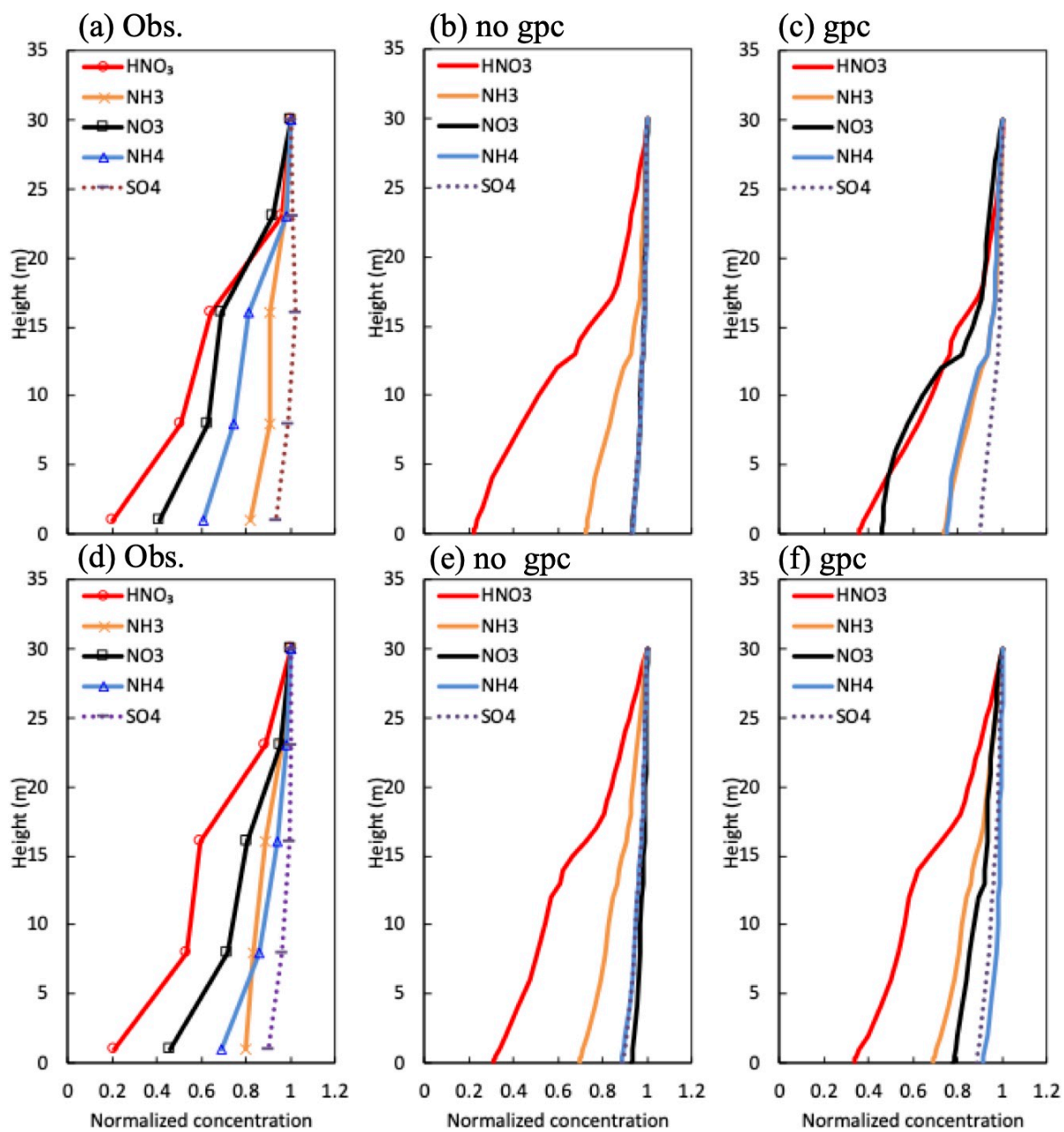


Figure 7. Mean vertical profiles in (a) observed and (b) calculated normalized mass concentration in the "no gpc" scenario and (c) the "gpc" scenario for HNO₃ and NH₃ gases and SO₄²⁻, NO₃⁻ and NH₄⁺ fine particles (a-c) during the daytime and (d-f) nighttime from 27 September to 11 October 2016.

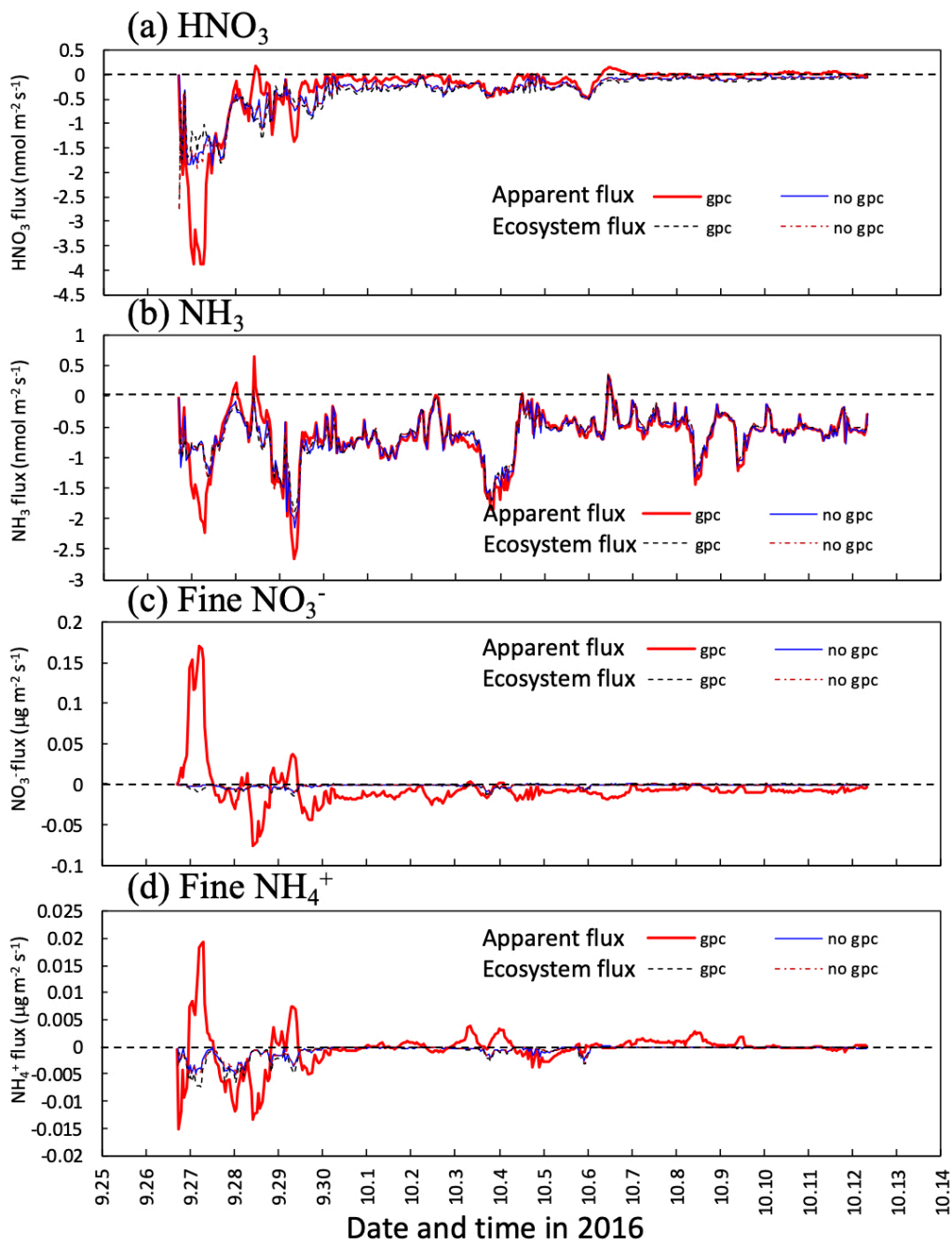


Figure 8. Temporal changes in calculated apparent mass flux of (a) HNO_3 gas and (b) NO_3^- and NH_4^+ fine particles at 30 m height in two scenarios ("gpc" and "no gpc") from 27 September to 11 October 2016. Fluxes captured by forest (ecosystem flux) are plotted in the figure.

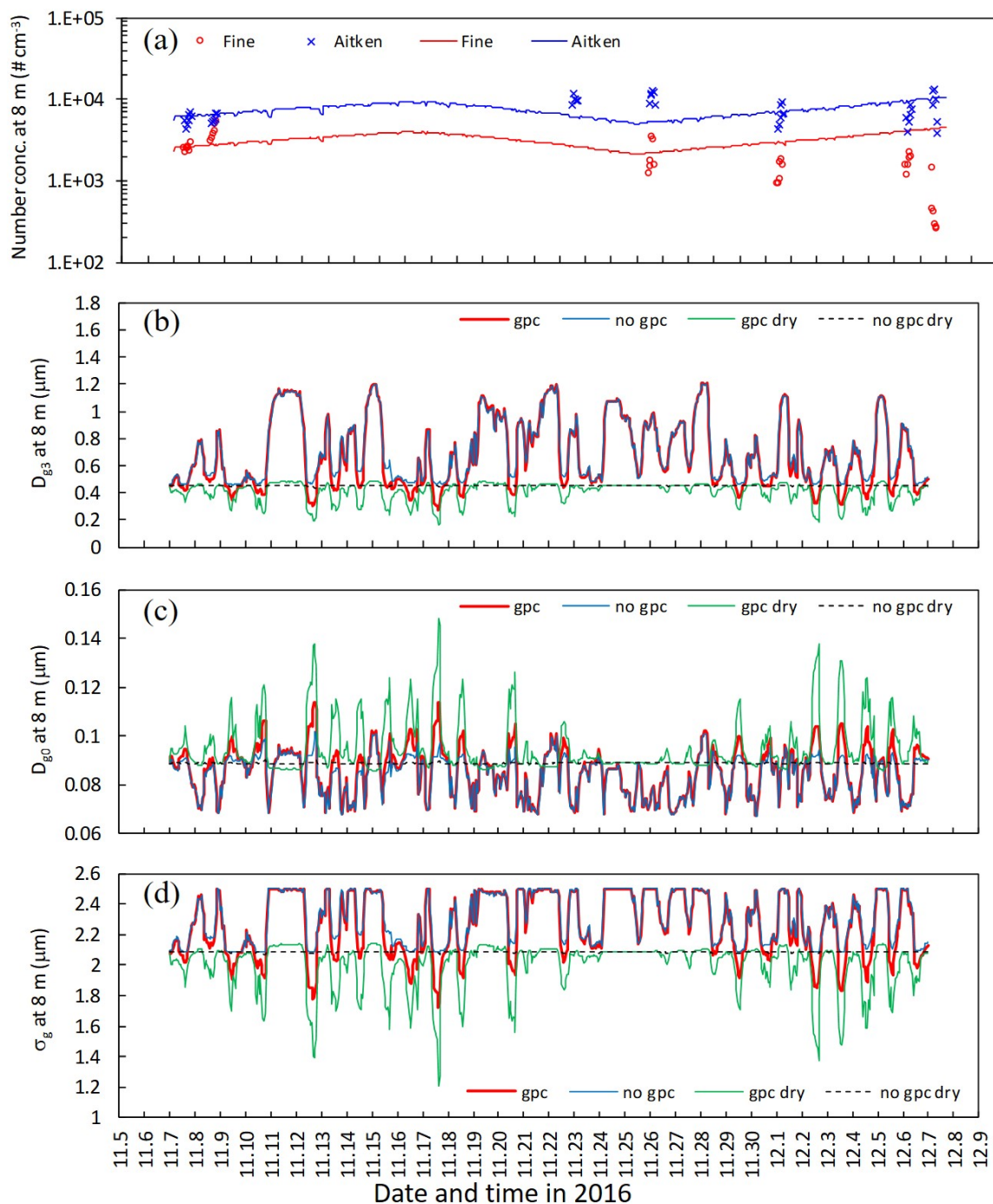


Figure 9. Temporal changes in (a) observed and calculated number concentration of fine and Aitken modes, and (b) calculated mass-equivalent (D_{g3}) and (c) number-equivalent geometric mean wet diameter (D_{g0}), and (d) standard deviation (σ_g) of fine particles at 8 m height from 7 November to 7 December 2016. Calculations for four scenarios ("gpc", "no gpc", "gpc dry", and "no gpc dry") are plotted in the figure.

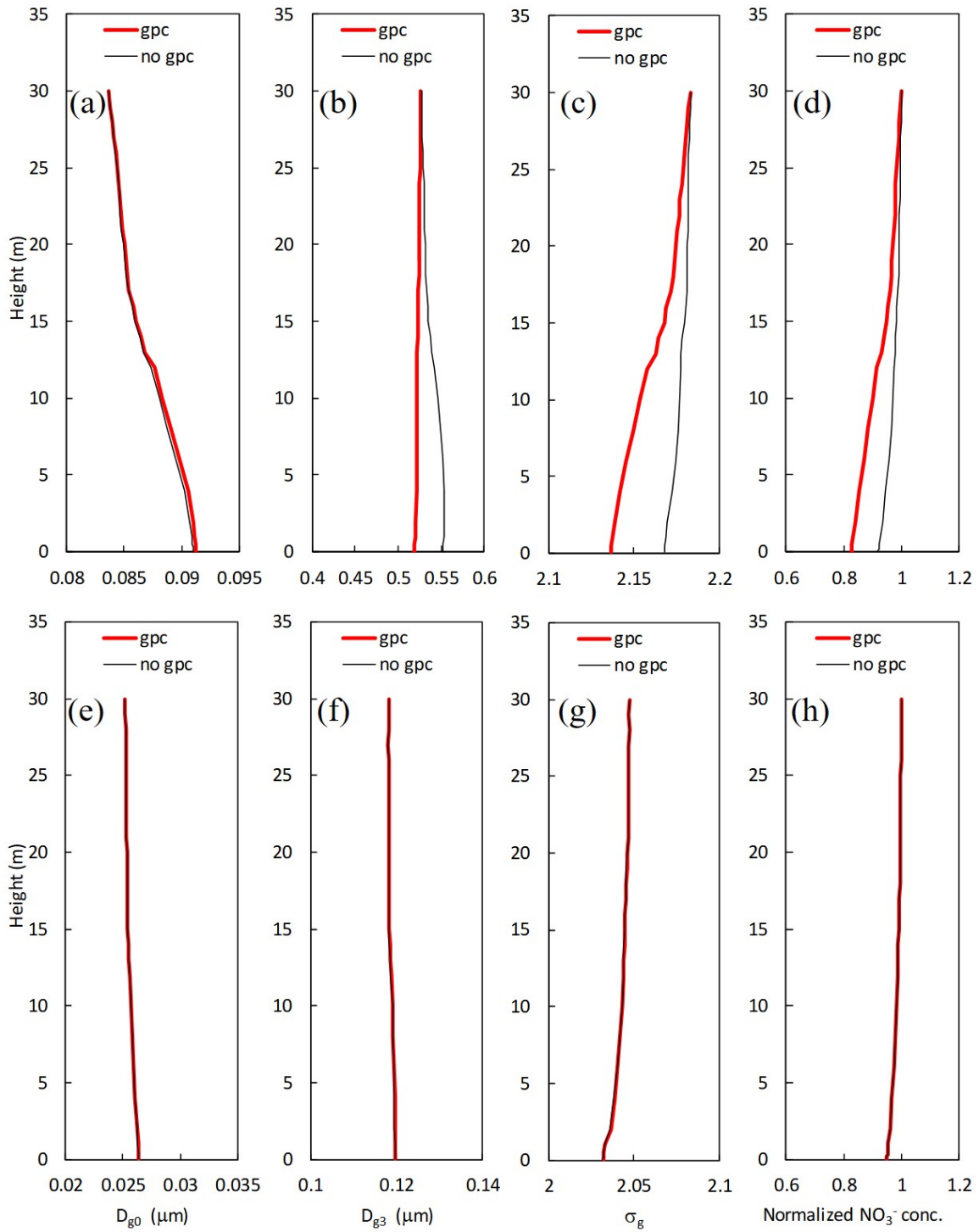


Figure 10. Mean vertical profiles for calculated (a, e) number-equivalent (D_{g0}) and (b, f) mass-equivalent geometric mean wet diameter (D_{g3}), (c, g) standard deviation (σ_g), and (d, h) normalized mass concentration of NO_3^- for (a-d) fine and (e-h) Aitken modes in two scenarios ("gpc" and "no gpc") from 7 November to 7 December 2016.

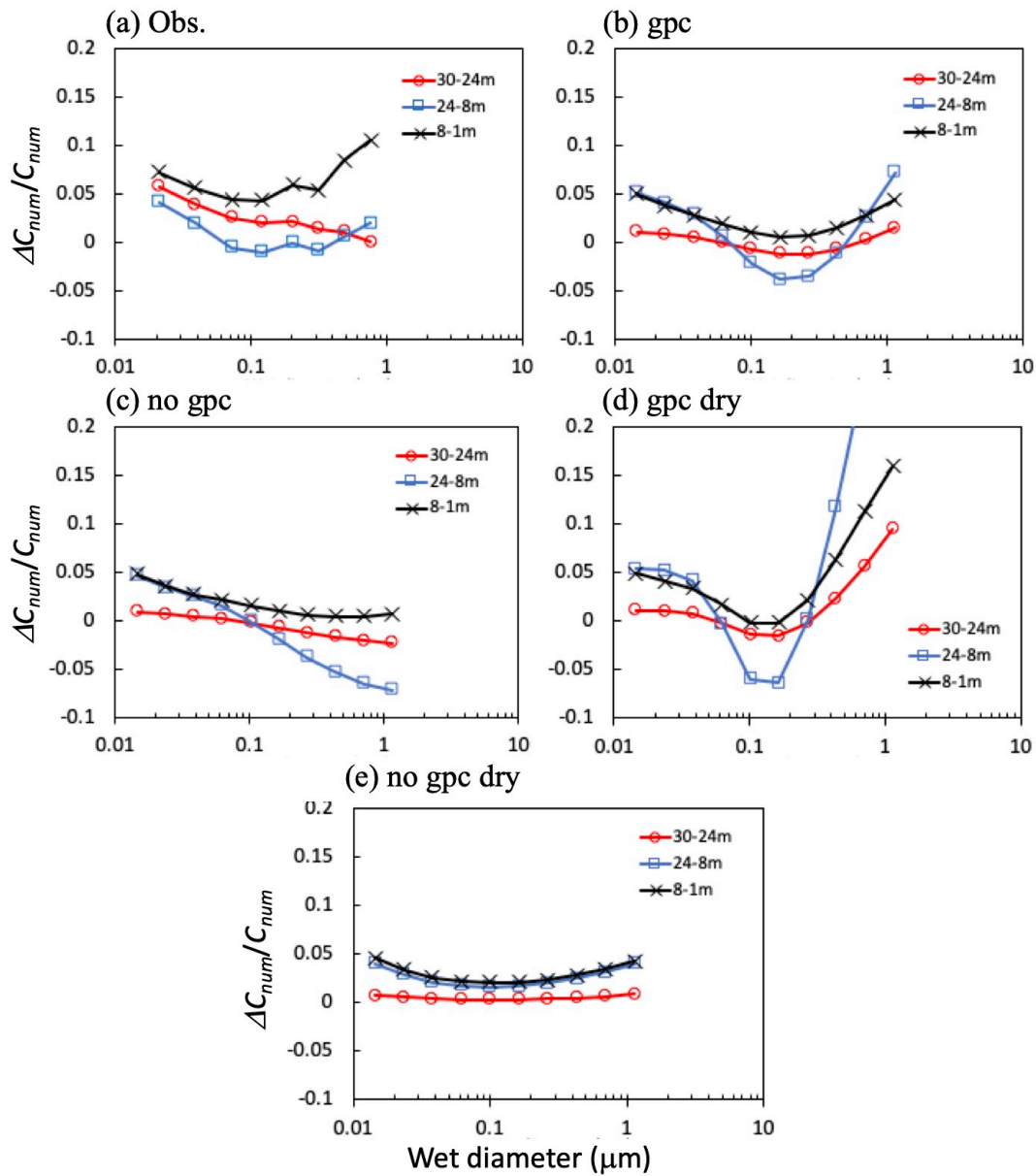


Figure 11. Differences (ΔC_{num}) in (a) observed and (b-e) calculated mean total number concentration (C_{num}) between height pairs for 11:00 -17:00 on 7, 8, 25, and 30 November 2016. Four calculation scenarios are presented in the figure: (b) "gpc", (c) "no gpc", (d) "gpc dry", and (e) "no gpc dry".

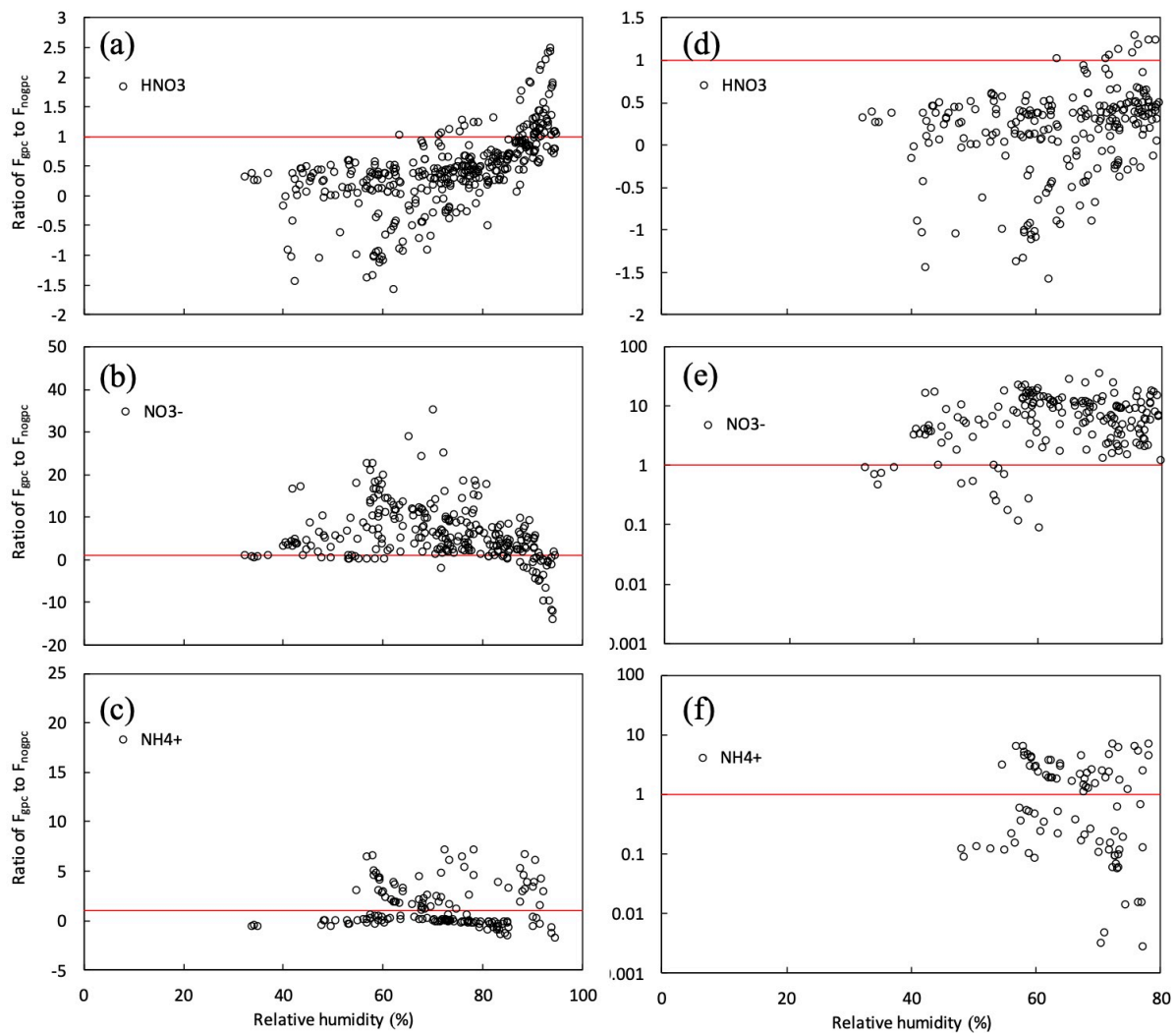


Figure 12. Relationship between relative humidity (RH) at 30 m height and "gpc" to "no gpc" ratios of calculated half-hourly fluxes (F_{gpc}/F_{nogpc}) of (a, d) HNO_3 gas and (b, e) NO_3^- and (c, f) NH_4^+ fine particles over the canopy from 27 September to 11 October 2016. Red lines represent the situation in which $F_{gpc} = F_{nogpc}$. (d) through (f) plot the same variables as (a) through (c), but under dry conditions ($RH < 80\%$).

Table 1. Summary of input data, and initial and boundary conditions for SOLVEG simulation setup; FP: filter-pack measurements, ELPI+: ELPI+ measurements, f_{io} : the volume fraction of inorganic compounds. It should be noted that the gaps between FP in rain days of the early autumn period were linearly incorporated for simulations.

	Early autumn	Late autumn
Period	26 September-11 October 2016	7 November-7 December 2016
Target of simulation	Fine inorganic mass concentration/flux	Total number concentration/flux
Upper boundary condition		
Inorganic mass concentration	FC Day/night (without rain days)	FC Weekly (continuous)
Particle size distribution	Fitting of ELPI+ (Fig. 1a)	
f_{io}	FC and Hachiouji station	FC and ELPI+